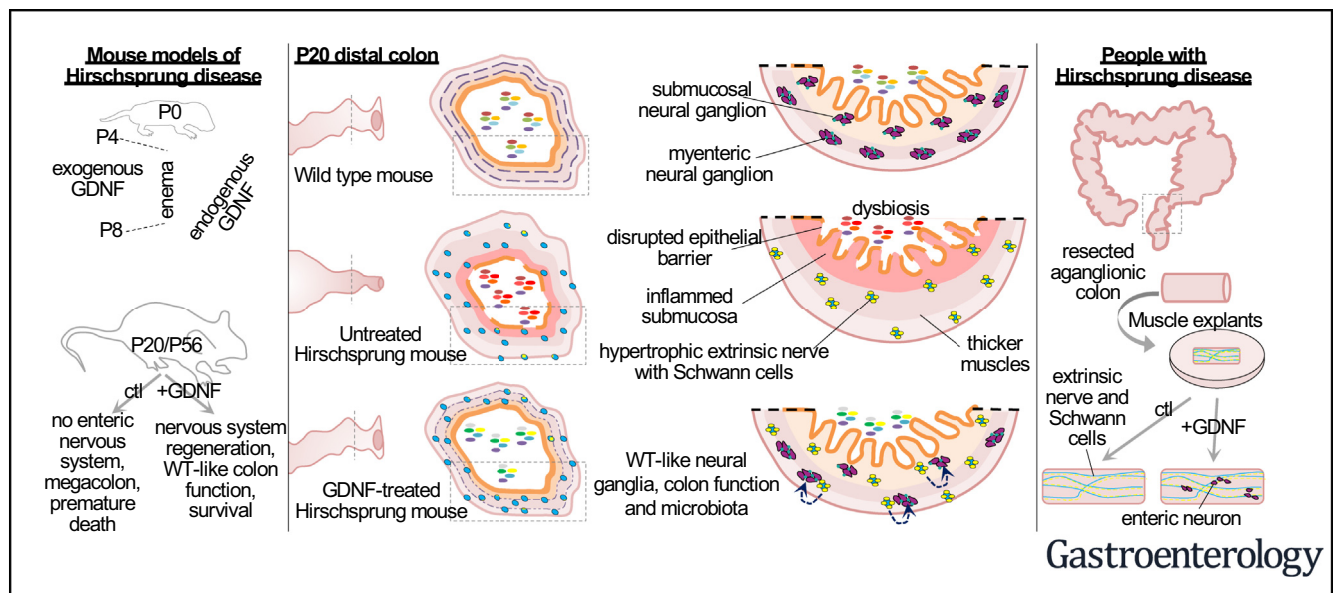




# Glial Cell-Derived Neurotrophic Factor Induces Enteric Neurogenesis and Improves Colon Structure and Function in Mouse Models of Hirschsprung Disease

Rodolphe Soret,<sup>1,2</sup> Sabine Schneider,<sup>3</sup> Guillaume Bernas,<sup>1</sup> Briana Christophers,<sup>3</sup> Ouliana Souchkova,<sup>1,2</sup> Baptiste Charrier,<sup>1,2</sup> Franziska Righini-Grunder,<sup>4</sup> Ann Aspirot,<sup>5,6</sup> Mathieu Landry,<sup>1</sup> Steven W. Kemel,<sup>1,2</sup> Christophe Faure,<sup>2,4,6</sup> Robert O. Heuckeroth,<sup>3</sup> and Nicolas Pilon<sup>1,2,6</sup>

<sup>1</sup>Département des Sciences Biologiques, Université du Québec à Montréal (UQAM), Montréal, Québec, Canada; <sup>2</sup>Centre d'excellence en recherche sur les maladies orphelines—Fondation Courtois (CERMO-FC), Université du Québec à Montréal, Montréal, Québec, Canada; <sup>3</sup>Department of Pediatrics, the University of Pennsylvania Perelman School of Medicine and The Children's Hospital of Philadelphia Research Institute, Philadelphia, Pennsylvania; <sup>4</sup>Division de gastroentérologie, hépatologie et nutrition pédiatrique, Centre Hospitalier Universitaire Sainte-Justine, Montréal, Québec, Canada; <sup>5</sup>Division de chirurgie pédiatrique, Centre hospitalier universitaire Sainte-Justine, Montréal, Québec, Canada; and <sup>6</sup>Département de pédiatrie, Université de Montréal, Montréal, Québec, Canada



**BACKGROUND & AIMS:** Hirschsprung disease (HSCR) is a life-threatening birth defect in which the distal colon is devoid of enteric neural ganglia. HSCR is treated by surgical removal of aganglionic bowel, but many children continue to have severe problems after surgery. We studied whether administration of glial cell derived neurotrophic factor (GDNF) induces enteric nervous system regeneration in mouse models of HSCR. **METHODS:** We performed studies with four mouse models of HSCR: *Holstein* ( $Hol^{Tg/Tg}$ , a model for trisomy 21-associated HSCR), *TashT* ( $TashT^{Tg/Tg}$ , a model for male-biased HSCR), *Piebald-lethal* ( $Ednrb^{s-1/s-1}$ , a model for *EDNBRB* mutation-associated HSCR), and *Ret*<sup>9/-</sup> (with aganglionosis induced by mycophenolate). Mice were given rectal enemas containing GDNF or saline (control) from postnatal days 4 through 8. We measured survival times of mice, and colon tissues were analyzed by histology, immunofluorescence, and immunoblots. Neural ganglia regeneration and structure, bowel motility,

epithelial permeability, muscle thickness, and neutrophil infiltration were studied in colon tissues and in mice. Stool samples were collected, and microbiomes were analyzed by 16S rRNA gene sequencing. Time-lapse imaging and genetic cell-lineage tracing were used to identify a source of GDNF-targeted neural progenitors. Human aganglionic colon explants from children with HSCR were cultured with GDNF and evaluated for neurogenesis. **RESULTS:** GDNF significantly prolonged mean survival times of  $Hol^{Tg/Tg}$  mice,  $Ednrb^{s-1/s-1}$  mice, and male  $TashT^{Tg/Tg}$  mice, compared with control mice, but not  $Ret^{9/-}$  mice (which had mycophenolate toxicity). Mice given GDNF developed neurons and glia in distal bowel tissues that were aganglionic in control mice, had a significant increase in colon motility, and had significant decreases in epithelial permeability, muscle thickness, and neutrophil density. We observed dysbiosis in fecal samples from  $Hol^{Tg/Tg}$  mice compared with feces from wild-type mice; fecal microbiomes of mice given

GDNF were similar to those of wild-type mice except for *Bac-teroides*. Exogenous luminal GDNF penetrated aganglionic colon epithelium of *Hol<sup>Tg/Tg</sup>* mice, inducing production of endogenous GDNF, and new enteric neurons and glia appeared to arise from Schwann cells within extrinsic nerves. GDNF application to cultured explants of human aganglionic bowel induced proliferation of Schwann cells and formation of new neurons. **CONCLUSIONS:** GDNF prolonged survival, induced enteric neurogenesis, and improved colon structure and function in 3 mouse models of HSCR. Application of GDNF to cultured explants of aganglionic bowel from children with HSCR induced proliferation of Schwann cells and formation of new neurons. GDNF might be developed for treatment of HSCR.

**Keywords:** Endogenous Stem Cells; In Situ Regeneration; NCAM; RET.

The enteric nervous system (ENS) extends along the entire gastrointestinal tract to control bowel motility and epithelial activity in response to sensory stimuli.<sup>1</sup> Interconnected enteric ganglia containing neurons and glia develop from neural crest-derived progenitors before birth. Incomplete colonization of distal colon by these ENS progenitors causes Hirschsprung disease (HSCR), a condition affecting 1 in 5000 newborns.<sup>2</sup> In HSCR, the distal colon without ganglia (ie, aganglionic colon) remains tonically contracted, causing functional intestinal obstruction. Symptoms also include bowel inflammation and a high risk of sepsis and premature death.<sup>2</sup>

HSCR is subdivided into short-segment (S-HSCR) and long-segment (L-HSCR) forms.<sup>2</sup> In S-HSCR (>80% of cases), the ENS is absent from the rectum and sigmoid colon only. L-HSCR means longer regions of distal bowel are aganglionic. Many genes influence HSCR risk,<sup>2</sup> and genetic risk variants may combine with nongenetic factors.<sup>3</sup> The major HSCR-associated gene is *RET*, a transmembrane tyrosine kinase activated when glial cell-derived neurotrophic factor (GDNF) binds the coreceptor GDNF family receptor  $\alpha$ -1 (*GFR $\alpha$ 1*). GDNF-*GFR $\alpha$ 1*-*RET* signaling is needed for survival, proliferation, and migration of ENS progenitors.<sup>4-6</sup> Accordingly, >90% of children with S-HSCR bear noncoding variants that reduce *RET* expression.<sup>7</sup> Protein-altering *RET* variants are not common in S-HSCR, but occur in ~35% of people with L-HSCR.<sup>8,9</sup> Other genes influencing HSCR risk encode EDNRB signaling pathway molecules, transcription factors, guidance and extracellular matrix molecules, and diverse additional factors.<sup>7,9-11</sup> Male sex also increases HSCR risk ~4-fold, whereas Down's syndrome increases HSCR risk ~100-fold.<sup>2</sup> Collectively, these observations mean that most children with HSCR have reduced but not absent *RET* signaling and that diverse additional factors impact HSCR occurrence.

Since 1948, surgical removal of aganglionic bowel has been life-saving for most children with HSCR.<sup>12</sup> However, postsurgical complications are common and can be long-lasting, impacting survival and quality of life.<sup>2</sup> One ideal alternative approach would be to rebuild the ENS and reduce the need for surgery. This idea prompted many

## WHAT YOU NEED TO KNOW

### BACKGROUND AND CONTEXT

Hirschsprung disease (HSCR) is a life-threatening birth defect in which distal colon is devoid of enteric neural ganglia. HSCR is treated by surgical removal of aganglionic bowel, but many children continue to have severe problems after surgery.

### NEW FINDINGS

GDNF prolonged survival, induced intestinal neurogenesis, and improved colon structure and function in 3 mouse models of HSCR. Application of GDNF to cultured explants of aganglionic bowel from children with HSCR also induced formation of new neurons.

### LIMITATIONS

Most of these studies were performed in mice; clinical studies are needed.

### IMPACT

GDNF might be developed for treatment of HSCR, but further studies are needed.

groups to develop cell transplantation-based HSCR therapies.<sup>13</sup> However, despite many encouraging results, some difficulties remain.<sup>14</sup> The optimal source of stem cells, ideal amplification, and differentiation strategies before transplantation, methods of cell delivery, and cell fate after transplantation are not yet well defined.

Here we tested the hypothesis that endogenous ENS progenitors could be activated after birth and generate enteric neurons de novo. Our cell-free strategy is based on the idea that HSCR is due to incomplete rostrocaudal colonization of the distal bowel by the main subpopulation of ENS progenitors, namely neural crest cells of vagal origin.<sup>15</sup> Because extracellular matrix in colon becomes refractory to migration after a certain developmental window,<sup>16</sup> reactivating vagal-derived ENS progenitor migration seemed unlikely after birth. However, it seemed possible that ENS progenitors of sacral<sup>17</sup> or Schwann cell lineage<sup>18</sup> origin, which are already present in the aganglionic colon, could be induced to proliferate and differentiate into functioning neurons. Schwann cells, in particular, are abundant in hypertrophic extrinsic nerve tracts that populate both muscular and submucosal layers of distal aganglionic bowel.<sup>19</sup> GDNF appeared as a primary candidate for postnatal reactivation of ENS progenitors in the aganglionic zone

**Abbreviations used in this paper:** EdU, 5-ethynyl-2'-deoxyuridine; ENS, enteric nervous system; *GFR $\alpha$ 1*, GDNF family receptor alpha-1; GDNF, glial cell-derived neurotrophic factor; HSCR, Hirschsprung disease; L-HSCR, long-segment Hirschsprung disease; NCAM, neural cell adhesion molecule; P, postnatal day; PFA, paraformaldehyde; PBS, phosphate-buffered saline; RFP, red fluorescent protein; S-HSCR, short-segment Hirschsprung disease; WT, wild-type; YFP, yellow fluorescent protein.

### Most current article

© 2020 by the AGA Institute. Published by Elsevier Inc. This is an open access article under the CC BY-NC-ND license (<http://creativecommons.org/licenses/by-nc-nd/4.0/>).

0016-5085

<https://doi.org/10.1053/j.gastro.2020.07.018>

notably because of its ability to stimulate migration and proliferation of Schwann cells in a RET-independent but GFR $\alpha$ 1-dependent manner through its alternative receptor neural cell adhesion molecule (NCAM).<sup>20,21</sup>

## Materials and Methods

### Mice

Details about all mouse lines used are in the [Supplementary Methods](#). Enema treatments of most mouse lines were performed at Université du Québec à Montréal, except for *Ret*<sup>9/-</sup> that were treated with mycophenolate<sup>22</sup> and GDNF at the Children's Hospital of Philadelphia Research Institute (as detailed in the [Supplementary Methods](#)). Where indicated, some *Hol*<sup>Tg/Tg</sup> and *Ednrb*<sup>s-1/s-1</sup> were also GDNF treated at the Children's Hospital of Philadelphia Research Institute after reciprocal exchange of mice between Philadelphia and Montreal. Unless specified otherwise (see [Supplementary Figure 1](#)), 10- $\mu$ L enemas consisting of a 1  $\mu$ g/ $\mu$ L solution of human recombinant GDNF (cat. #450-10, PeproTech, Cranbury, NJ) diluted in phosphate-buffered saline (PBS) were administered daily between postnatal day (P) 4 to P8 (see [Supplementary Methods](#) for more detail). Clinical-grade GDNF (Medgenesis Therapeutix Inc, Victoria, BC, Canada) and a previously described 6XHis-tagged version<sup>23</sup> used for some experiments had similar efficiency (see [Supplementary Methods](#) for other tested molecules). For 5-ethynyl-2-deoxyuridine (EdU) incorporation assays, mouse pups received 10- $\mu$ L intraperitoneal injections of a 10 mmol/L EdU solution (Cat. # C10337; Thermo Fisher Scientific, Waltham, MA) once a day during the 5-day (P4 to P8) GDNF enema treatment.

### Tissue Processing, Staining, and Imaging

Bowel was cut longitudinally along the mesentery, washed in PBS saline, pinned onto Sylgard-coated (Dow Corning, Freeland, MI) Petri dishes, fixed with 4% paraformaldehyde (PFA) at 4°C overnight, and finally microdissected to separate longitudinal/circular muscles from the submucosa/mucosa layer. For ex vivo analyses of living tissues, unfixed tissues were microdissected in ice-cold oxygenated Krebs solution. For histologic analyses, fixed full-thickness bowel segments were embedded in paraffin and transversally sectioned at 10  $\mu$ m. For Western blotting, unfixed organs were weighed and dissolved in radioimmunoprecipitation assay buffer, using 1 mL for every 100 mg of tissue (further details are provided in the [Supplementary Methods](#)). Details about immunofluorescence and imaging can be found in the [Supplementary Methods](#).

### Analysis of Colonic Motility and Permeability

In vivo analysis of distal colonic motility in P20 mice was performed using the bead latency test, as detailed in the [Supplementary Methods](#). For ex vivo analysis of colonic motility, strips of living muscles from most distal colon (1 cm from the anus) of P20 mice were prepared as described above and attached in the longitudinal direction in a Schuler organ bath (Harvard Apparatus, Holliston, MA) filled with oxygenated Krebs solution. Contraction/relaxation of longitudinal muscles was then recorded as detailed in the [Supplementary Methods](#). For ex vivo analysis of mucosal barrier function, segments of living mucosa from the most distal colon of P20 mice were

prepared as described above, mounted in Ussing chambers with 0.5 cm<sup>2</sup> exposed surface area (Model U-9926; Warner Instruments, Hamden, CT), and evaluated for paracellular permeability as described in the [Supplementary Methods](#).

### Microbiome Analysis

Stool isolation, microbiome sequencing, and data analysis were performed as previously described<sup>24</sup> (details are provided in the [Supplementary Methods](#)).

### Ex Vivo Time-Lapse Imaging and Culture of Murine Aganglionic Colon

For time-lapse imaging, strips of living muscles from the last centimeter of distal colon from P4 *Hol*<sup>Tg/Tg</sup>;G4-RFP (red fluorescent protein) double-transgenic pups were prepared as described above and pinned onto Sylgard-coated 35-mm ibidi  $\mu$ -dishes (Cat. #81156; ibidi USA, Fitchburg, WI). Muscle strips were then cultured in suspension as detailed in the [Supplementary Methods](#). For ex vivo induction of neurogenesis, strips of living muscles from the last centimeter of distal colon from P4 *Hol*<sup>Tg/Tg</sup> pups were cultured as for time-lapse imaging in the presence of 0.5  $\mu$ mol/L EdU. After 96 hours of culture, tissues were fixed with PFA and processed for immunofluorescence and EdU labeling.

### Culture of Human Aganglionic Colon Tissues

Human sigmoid colon tissue was obtained from 12 HSCR patients undergoing Swenson-type surgical resection of the aganglionic zone. Nine patients (7 boys and 2 girls; aged between 28 and 1638 days at the time of surgery) were recruited at the Centre hospitalier universitaire Sainte-Justine (Montreal, QC, Canada), and 3 patients (2 boys and 1 girl; aged between 300 and 1177 days at the time of surgery) were recruited at the Children's Hospital of Philadelphia. After the surgery, full-thickness colon tissues were placed in ice-cold Krebs solution or Belzer's UW Cold Storage Solution (Bridge to Life Ltd, Columbia, SC) and immediately brought to the relevant research laboratory.

Muscle strips were then prepared as described above and cut in smaller pieces of 0.5 cm  $\times$  0.5 cm. One piece was kept aside for validation of aganglionosis via immunofluorescence, and the others were cultured for 96 hours as described above for inducing neurogenesis in mouse tissues. Samples from 2 patients (86 and 1638 days of age at surgery) were in addition cultured for 7 days, under the same conditions. At the end of the culture period, all tissues were fixed with PFA and processed for immunofluorescence and EdU labeling.

### Study Approval

All experiments with mice were approved by animal research ethics committees of the Université du Québec à Montréal (CIPA reference #878) and the Children's Hospital of Philadelphia Research Institute (IAC reference #16-001041). Likewise, experiments with human samples were approved by human research ethics committees of the Université du Québec à Montréal (CIEREH protocol #491), the Centre hospitalier universitaire Sainte-Justine (CER protocol #4172), and the Children's Hospital of Philadelphia (Institutional Review Board protocol #13-010357). Informed consent for the collection and

use of human tissues was obtained from all donors, and parents or legal guardian, except for 1 piece of deidentified human colon.

## Statistics

All experiments used a minimum of 3 biological replicates. Where relevant, the exact number of independent replicates (n) and statistical tests used to calculate *P* values are included in figures or legends, or both. *P* values were determined using GraphPad Prism 6 (GraphPad Prism Software, San Diego, CA) with the exception of microbiome data, which were analyzed with R software (The R Foundation for Statistical Computing, Vienna, Austria).

## Results

### Glial Cell-Derived Neurotrophic Factor Enemas Rescue Aganglionosis in 3 Mouse Models of Short-Segment Hirschsprung Disease

Using rectal enemas, we tested whether early postnatal administration of GDNF could enhance survival of 4 mouse models of S-HSCR: *Holstein* ( $Hol^{Tg/Tg}$ ), a fully penetrant model for trisomy 21 (collagen VI overexpression)-associated HSCR<sup>25</sup>; *TashT* ( $TashT^{Tg/Tg}$ ), a partially penetrant model for male-biased HSCR<sup>26</sup>; *Piebald-lethal* ( $Ednrb^{s-l/s-l}$ ), a fully penetrant model for *EDNRB* mutation-associated HSCR<sup>27</sup>; and *Ret*<sup>9-/-</sup> mutant mice, a hypomorphic model where aganglionosis is induced by mycophenolic acid.<sup>22</sup> The enema volume necessary to fill the whole colon, GDNF concentration, treatment time window, as well as duration and frequency of therapy were first empirically determined with  $Hol^{Tg/Tg}$  pups (Supplementary Figure 1A–E).

Remarkably, our selected treatment (ie, daily administration of 10  $\mu$ g GDNF in PBS as 10- $\mu$ L enemas for 5 consecutive days between P4 and P8) prevented death in about half of the  $Hol^{Tg/Tg}$  mice at P28, the maximum age of survival for control  $Hol^{Tg/Tg}$  mice (Figure 1A). Most animals surviving to P28 reached adult age after GDNF treatment, and mice evaluated could reproduce (2 tested breeding pairs were fertile). The few animals that were allowed to survive beyond P56 (our adult reference age) eventually died of megacolon or dystocia between P68 and P250 (Supplementary Figure 1C).

Importantly, the same GDNF enema treatment also prevented premature death for more than 60% of  $Ednrb^{s-l/s-l}$  mice (Figure 1, B) and for all male  $TashT^{Tg/Tg}$  pups (Figure 1C). Nine GDNF-treated male  $TashT^{Tg/Tg}$  mice kept for more than 1 year looked healthy, without any sign of adverse effects. Enema treatment of  $Hol^{Tg/Tg}$  mice using Noggin, endothelin-3, or the serotonin receptor (5-hydroxytryptamine receptor 4) agonist RS67506 (rationale provided in Supplementary Table 1) failed to increase life expectancy, suggesting specific benefit to GDNF (Supplementary Figure 1F). We also failed to further increase the overall survival rate of GDNF-treated  $Hol^{Tg/Tg}$  animals by replacing standard chow with a gel diet (Supplementary Figure 1G) or by combining GDNF with

vitamin C, serotonin, or endothelin 3 (Supplementary Table 1 and Supplementary Figure 1H).

Because modest reductions in RET function are common in people with HSCR, we wanted to determine whether GDNF enemas could work in RET hypomorphic mice. Unfortunately, there are no good mouse models for *RET* mutation-associated HSCR. *Ret*-null mice have total intestinal aganglionosis,<sup>28</sup> whereas *Ret* heterozygotes are overtly normal.<sup>4</sup> We therefore decided to use our established protocol to induce distal bowel aganglionosis in  $Ret^{9/-}$  hypomorphic mice using mycophenolate mofetil.<sup>22</sup> Surprisingly, far less prenatal mycophenolate was needed to cause dose-dependent aganglionosis in our novel experimental conditions (with *Ret* mutants rederived in a new animal facility) (Supplementary Figure 2A) compared with our prior studies,<sup>22</sup> and postnatal GDNF enemas did not improve survival compared with PBS alone (Supplementary Figure 2B). Instead, many pups died with distended bowel before the end of GDNF treatment, even at the lowest mycophenolate concentration (Supplementary Figure 2C). Moreover, many ill pups had ganglia throughout the bowel (Supplementary Figure 2D), suggesting highly variable efficiency of mycophenolate treatment and additional toxicity that complicates data interpretation.

To determine how GDNF enemas enhanced survival in the other 3 HSCR mouse models, we tested the hypothesis that GDNF induced postnatal neurogenesis in aganglionic distal colon. We focused on the *Holstein* line for practical reasons (fertility is low in *Piebald-lethal*, and megacolon incidence is lower in *TashT*), and analyzed P20 animals because  $Hol^{Tg/Tg}$  mice generally reach this stage even without enema treatment (Figure 1A). As we previously reported,<sup>25</sup> myenteric HuC/D<sup>+</sup> neurons and SOX10<sup>+</sup> glia were abundant in wild-type (WT) distal colon and absent from the last centimeter of  $Hol^{Tg/Tg}$  colon (Figure 2A). In contrast, in  $Hol^{Tg/Tg}$  distal colon, SOX10<sup>+</sup> cells were mainly within thick extrinsic nerve fibers (Figure 2A) where Schwann cells reside.<sup>18</sup> Remarkably, the distal colon from GDNF-treated  $Hol^{Tg/Tg}$  animals had numerous HuC/D<sup>+</sup> neurons and SOX10<sup>+</sup> glia organized into ganglia primarily adjacent to extrinsic nerves (Figure 2A and Supplementary Video 1). These GDNF-induced ganglia formed Tuj1<sup>+</sup> interconnected networks in both myenteric and submucosal plexuses (Figure 2B). Quantification of myenteric neuron density in the whole colon of  $Hol^{Tg/Tg}$  and male  $TashT^{Tg/Tg}$  mice showed GDNF effects are most prominent in the distal colon (ie, final 3 cm), with minor effects in the proximal colon (Figure 2A and Supplementary Figure 3). In the mid colon of GDNF-treated  $Hol^{Tg/Tg}$  mice, the increased neuron density (Figure 2A) was mainly due to an enlargement of preexisting myenteric ganglia (Supplementary Figure 3A). In the most distal colon, where untreated  $Hol^{Tg/Tg}$  mice are normally devoid of enteric neurons, GDNF-treated  $Hol^{Tg/Tg}$  mice had an average neuron density that was approximately 40% that of WT mice (Figure 2A). When neuron density in the distal colon was too low, GDNF-treated  $Hol^{Tg/Tg}$  mice developed megacolon (Supplementary Figure 1I). Remarkably, in GDNF-treated  $TashT^{Tg/Tg}$  males, neuron density in

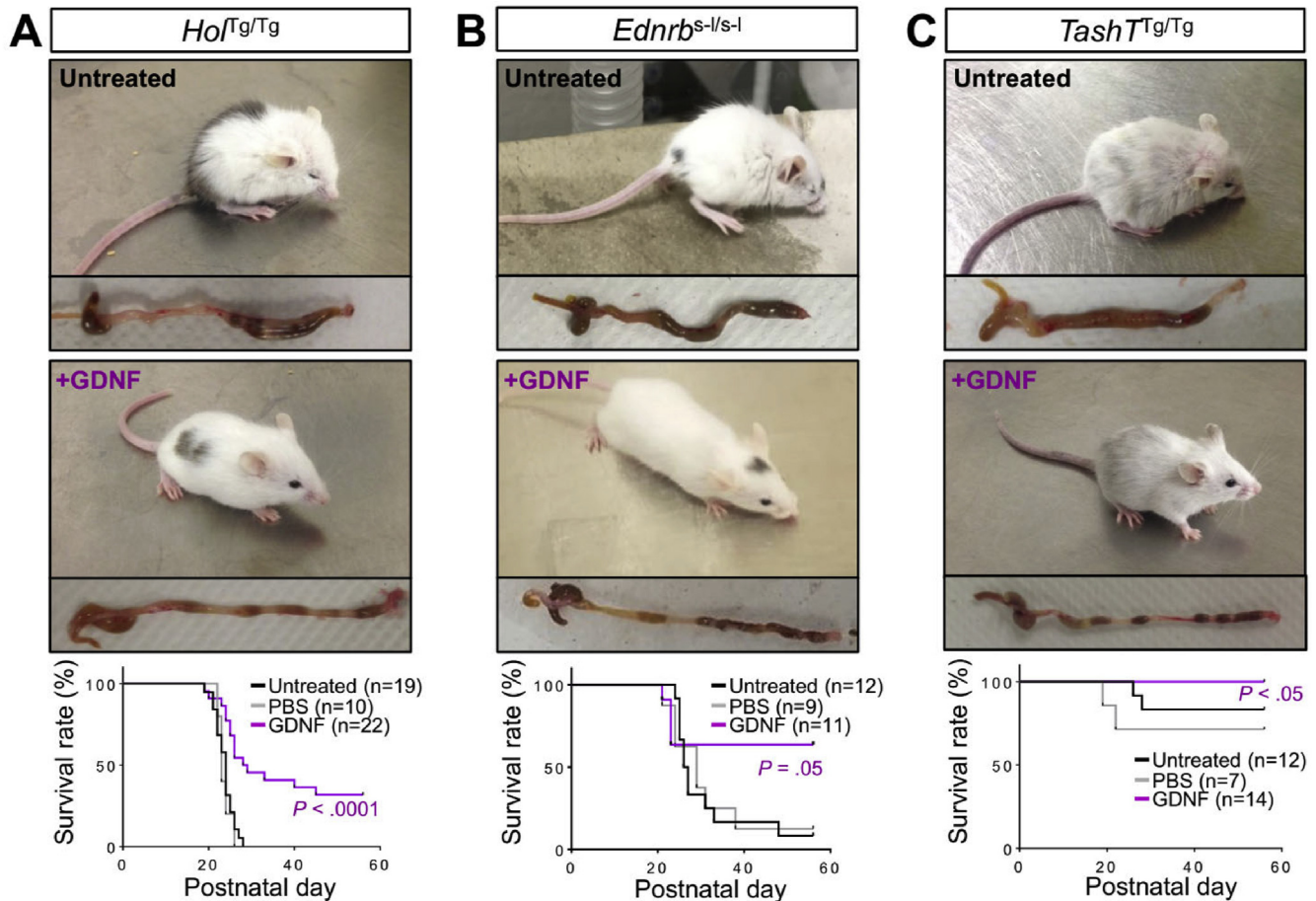


**Figure 1.** GDNF enemas rescue aganglionic megacolon in HSCR mouse models. Daily administration of GDNF enemas to (A) *Hoi<sup>Tg/Tg</sup>*, (B) *Ednrb<sup>S-/s-1</sup>*, and (C) *Tash<sup>Tg/Tg</sup>* mice between P4 and P8 positively impacts both megacolon symptoms and survival rates (Mantel-Cox statistical test, GDNF-treated vs PBS-treated groups).

the most distal colon was completely restored (Supplementary Figure 3B and C).

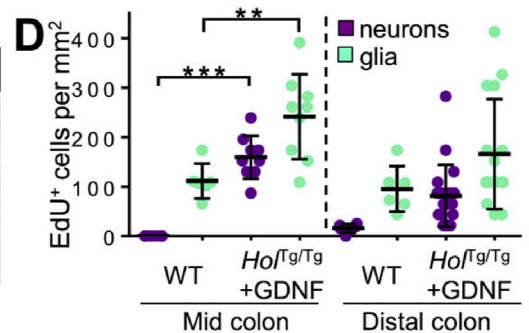
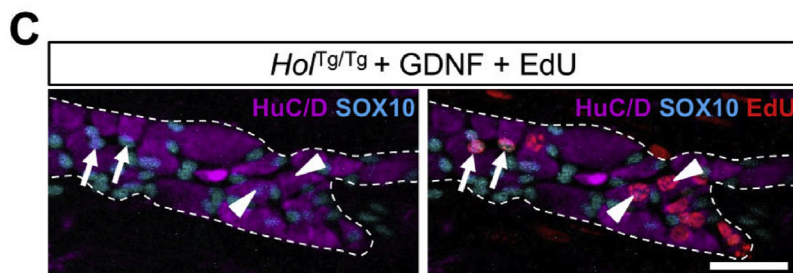
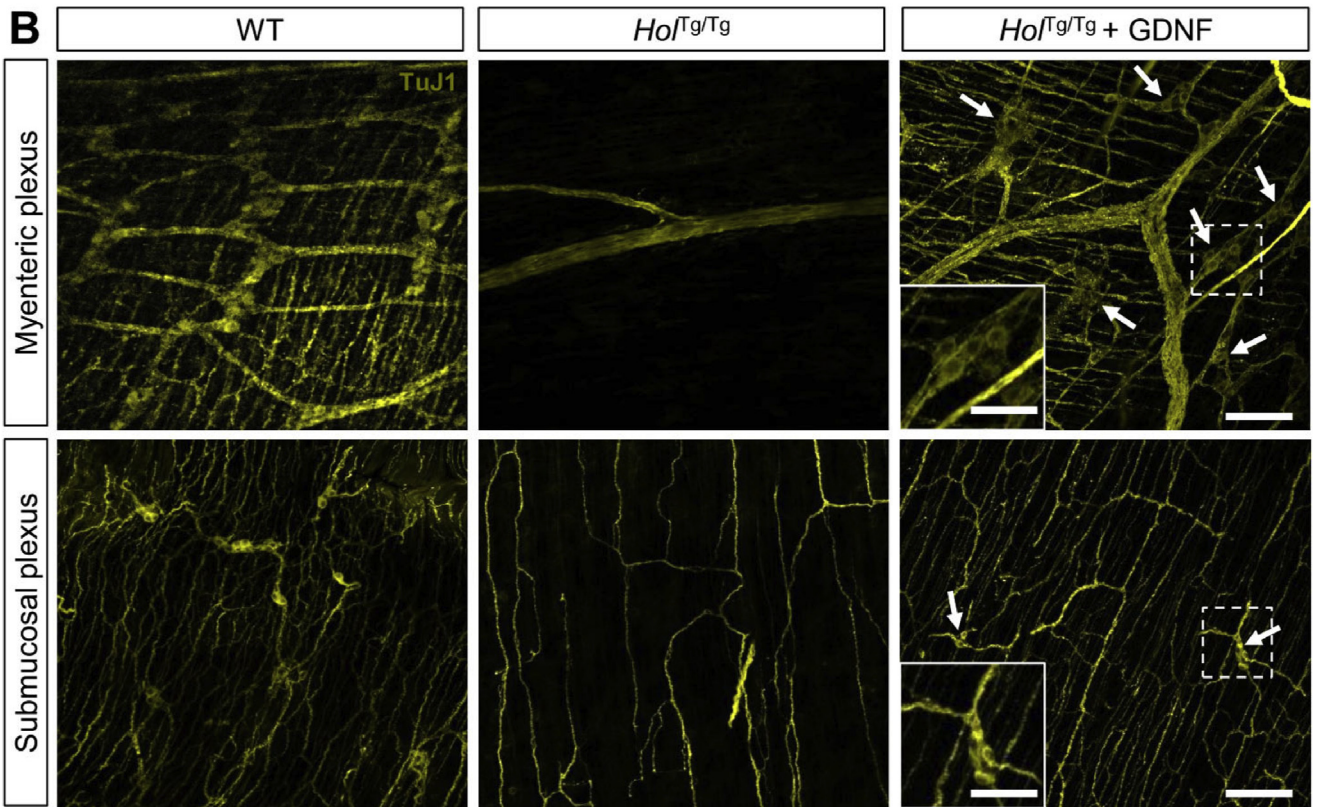
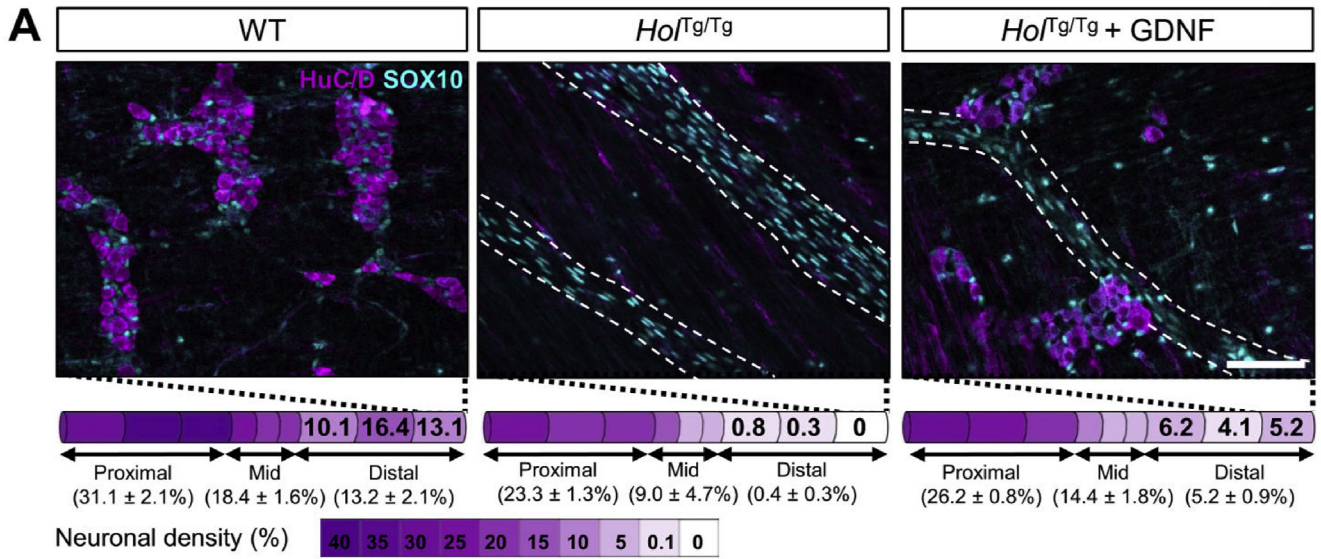
EdU incorporation assays confirmed that GDNF induced proliferation of neuron and glia progenitors during the 5-day treatment from P4 to P8. Staining of P20 *Hoi<sup>Tg/Tg</sup>* colon from mice that received daily EdU injections during GDNF treatment revealed many EdU<sup>+</sup> HuC/D<sup>+</sup> (presumptive neurons) and EdU<sup>+</sup> SOX10<sup>+</sup> (presumptive glia or neuron/glia progenitors) in both myenteric and submucosal ganglia (Figure 2C and D and Supplementary Figure 4). Yet, only a few, very small ganglia (ie, 3 neurons) were fully populated by EdU<sup>+</sup> neurons (Supplementary Figure 4C). Collectively these data suggest that GDNF enemas induce proliferation and differentiation of ENS progenitors in the distal colon and that some of induced neurons and glia cluster into new ganglia.

#### Glial Cell-Derived Neurotrophic Factor-Induced Enteric Nervous System Is Morphologically and Functionally Similar to Wild-Type

Again focusing on the *Hoi<sup>Tg/Tg</sup>* model, we next asked to what extent GDNF-induced ENS in the distal colon

resembles WT at P20. The average neuron-to-glia ratio within GDNF-induced myenteric ganglia was statistically similar to WT ( $P = .16$ ) (Figure 3A). Relative proportions of major myenteric neuron subtypes, including cholinergic (ChAT<sup>+</sup>) and nitroergic (nNOS<sup>+</sup>) neurons, were also very similar to WT (Figure 3B and C). Moreover, many other neuronal subtypes were detected, including TH<sup>+</sup> dopaminergic neurons, CaR<sup>+</sup> excitatory motor neurons, VIP<sup>+</sup> inhibitory motor neurons, and SubP<sup>+</sup> excitatory motor neurons (Figure 3C). Interestingly, in the proximal and mid colon of *Hoi<sup>Tg/Tg</sup>* mice (Supplementary Figure 5), GDNF treatment also corrected the imbalance of nitroergic (increased) and cholinergic (decreased) neuron subtypes that is observed proximal to the aganglionic segment in both HSCR mouse models and in patients.<sup>29-32</sup>

To evaluate function of P20 GDNF-induced myenteric ganglia, we analyzed colonic motility in vivo, using the bead latency test. In contrast to untreated *Hoi<sup>Tg/Tg</sup>* mice that never expelled a rectally inserted glass bead during our 30-minute observation period, a subset of GDNF-treated *Hoi<sup>Tg/Tg</sup>* expelled the bead in 10 to 21 minutes, a bit slower than WT mice (range, 2 to 8 minutes) (Figure 3D). Analysis of neuron density in these GDNF-treated *Hoi<sup>Tg/Tg</sup>* mice



revealed a robust inverse correlation between time to expel the bead and neuron density in the distal colon (Supplementary Figure 6A).

We also evaluated motility *ex vivo* using muscle strips from P20 distal colons attached to force transducers in organ baths. This system allows electric field stimulation-induced contractions of WT colon muscles to be slightly increased by inhibition of nitric oxide synthase with  $N^G$ -nitro-L-arginine methyl ester, which can then be robustly counteracted by inhibition of cholinergic signaling with atropine. Reminiscent of *in vivo* data, colon muscle strips from GDNF-treated  $Hol^{Tg/Tg}$  mice displayed 1 of 2 distinct response patterns (Figure 3E and Supplementary Figure 6B), similar to WT or similar to untreated  $Hol^{Tg/Tg}$ . To indirectly test function of P20 GDNF-induced submucosal ganglia, we analyzed epithelial permeability to small fluorescently labeled dextran molecules (FD4) in Ussing chambers. Once more, distal colonic tissues from GDNF-treated  $Hol^{Tg/Tg}$  mice displayed 2 distinct response types, with mucosa either impermeable to FD4 like WT tissues or permeable to FD4 like control  $Hol^{Tg/Tg}$  tissues from untreated mice (Figure 3F).

To complement ENS analyses, we evaluated other HSCR-associated bowel anomalies.  $Hol^{Tg/Tg}$  mouse colon had thicker smooth muscles and more neutrophils than WT mice, but GDNF-treated  $Hol^{Tg/Tg}$  mouse colon was similar to WT (Figure 3G–I and Supplementary Figure 7). Similarly, stool microbiome profiling demonstrated dysbiosis in P20  $Hol^{Tg/Tg}$  mouse colon, but average abundance of several bacterial genera in  $Hol^{Tg/Tg}$  mouse colon were indistinguishable from WT after GDNF treatment (Figure 3J). A notable exception was *Bacteroides* abundance, which was low in  $Hol^{Tg/Tg}$  mice and even lower after GDNF treatment. Accordingly, beta diversity analysis revealed distinct microbial communities among WT,  $Hol^{Tg/Tg}$ , and GDNF-treated  $Hol^{Tg/Tg}$  mice (Figure 3K).

### Schwann Cells Within Extrinsic Nerves Are a Target of Glial Cell-Derived Neurotrophic Factor in Aganglionic Colon

To elucidate how GDNF induces enteric neurogenesis, we first evaluated GDNF distribution in P8 bowel via Western blot, taking advantage of size differences between recombinant (15 kDa) and endogenous (20 kDa, glycosylated) GDNF monomers. Recombinant GDNF was detected in GDNF-treated  $Hol^{Tg/Tg}$  distal colon but not in proximal colon (Figure 4A). Surprisingly, while endogenous GDNF is

normally only detected in ileum, recombinant GDNF enemas triggered robust increases in endogenous GDNF throughout the colon (Figure 4A). Recombinant GDNF was no longer detected in colon nor in any other tissue at P20, suggesting that administered GDNF primarily acts during the treatment period (Supplementary Figure 8). To assess precise locations of recombinant GDNF during treatment, we treated  $Hol^{Tg/Tg}$  mice using a 6XHis-tagged version of GDNF<sup>23</sup> (HisGDNF). Time-course analysis of the distal colon 2 hours after GDNF treatment on P4, P6, and P8 revealed HisGDNF accumulated over time in colon submucosa (Figure 4B), smooth muscles, and subsets of enteric neurons (Figure 4C and Supplementary Figure 9) of  $Hol^{Tg/Tg}$  mice. Interestingly, RET levels also increased (Figure 4B and Supplementary Figure 9), supporting the hypothesis that GDNF-RET autoregulatory loops are activated in GDNF-treated colon. Remarkably, HisGDNF and RET were both detected in induced neurons close to extrinsic nerves of HisGDNF-treated animals, not only in  $Hol^{Tg/Tg}$  mice (Figure 4C) but also in *Ednrb<sup>s-1/s-1</sup>* mice (Supplementary Figure 10A), and in both of our mouse facilities in Montreal and Philadelphia (Supplementary Figure 10A and B).

Given that induced neurons and glia were often closely associated with extrinsic nerves, we hypothesized that nerve-associated Schwann cells might be GDNF-targeted ENS progenitors. We first assessed response of Schwann cells to GDNF using live explants of distal colon muscularis externa from P4  $Hol^{Tg/Tg};G4-RFP$  double-transgenic pups. In these mice, neural crest derivatives, including Schwann cells, are marked by RFP fluorescence.<sup>33</sup> Time-lapse imaging of explants after 72 hours of culture suggested GDNF (5  $\mu$ g/mL) stimulates both migration and proliferation of Schwann cells (Figure 4D and Supplementary Videos 2 and 3). The impact of GDNF on proliferation of these Schwann cells was confirmed via immunofluorescence after 96 hours of culture, which revealed a 3-fold increase in Ki67<sup>+</sup> SOX10<sup>+</sup> double-positive cells upon exposure to GDNF (Figure 4E and F).

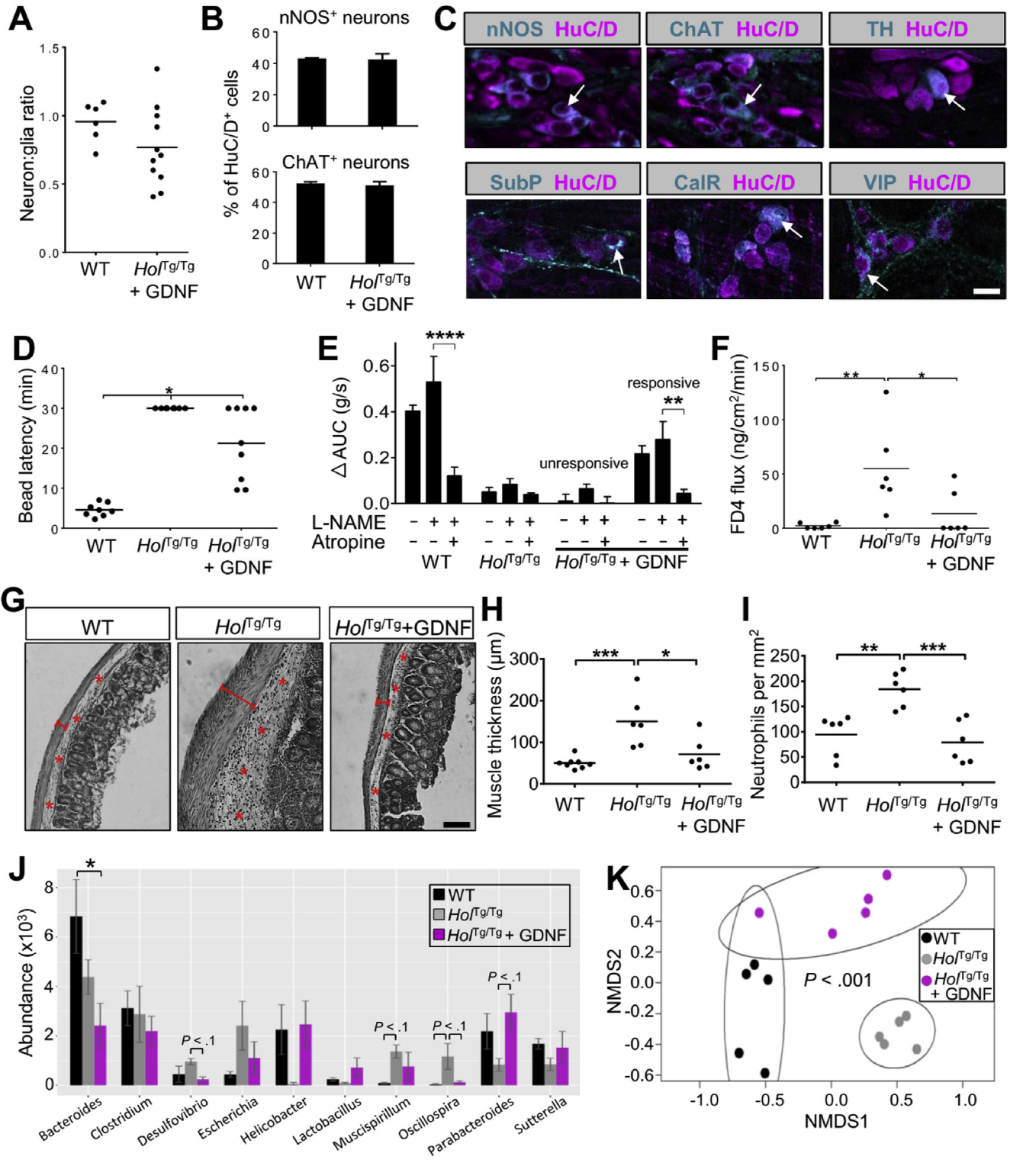
To more definitely demonstrate Schwann cells are GDNF targets, we used *in vivo* genetic cell lineage tracing with the Schwann lineage-specific *Dhh-Cre* driver and the  $R26^{[Floxed Stop]YFP}$  Cre reporter allele in the *Holstein* [FVB/N] mutant background. Analysis of proximal and mid colons from untreated  $Dhh-Cre^{Tg/+};R26^{YFP/+}$  and  $Hol^{Tg/Tg};Dhh-Cre^{Tg/+};R26^{YFP/+}$  animals at P20 showed that the proportion of Schwann cell lineage-derived (yellow fluorescent protein [YFP]<sup>+</sup>) myenteric neurons increased from 5% to 7% in a pure FVB/N genetic

**Figure 2.** GDNF enemas induce a new ENS in the otherwise aganglionic region of P20  $Hol^{Tg/Tg}$  mice. (A) GDNF treatment induces myenteric ganglia containing HuC/D<sup>+</sup> neurons and SOX10<sup>+</sup> glia. For each colon subregion (cylinders), average neuronal density (color coded) is expressed as the percentage of the area occupied by HuC/D<sup>+</sup> cells in the myenteric plexus (n = 6 mice per group; 3 fields of view per subregion). (B) Immunofluorescence analysis of TuJ1<sup>+</sup> neuronal structures in myenteric and submucosal plexus, including GDNF-induced ganglia (arrows). Insets are zoomed-in views of dashed boxes. (C) EdU incorporated in GDNF-induced myenteric neurons (arrowheads) and glia (arrows) during the 5-day treatment. (D) Quantitative results of panel C are expressed as the number of EdU<sup>+</sup> cells per mm<sup>2</sup> (n = 3 WT and 3 GDNF-treated  $Hol^{Tg/Tg}$  mice; 2 to 7 fields of view per animal. \*\**P* < .01; \*\*\**P* < .001; 1-way analysis of variance with post hoc Sidak's test. All images show a z-stack projection representative of observations made from 3 mice. The dashed outlines delineate (A) extrinsic nerve fibers or (C) a single ganglion. Scale bars, 100  $\mu$ m (A and B) and 50  $\mu$ m (B insets, and C).

background to 10% to 11% in the presence of homozygous *Holstein* mutation (Supplementary Figure 11A and B). Remarkably, the Schwann cell lineage contribution further increased to 34% of myenteric neurons in the distal colon of GDNF-treated *Hol<sup>Tg/Tg</sup>;Dhh-Cre<sup>Tg/+</sup>;R26<sup>YFP/+</sup>* animals (Figure 4G and H). By daily EdU administration during GDNF treatment, we identified 4 subgroups of induced

myenteric neurons based on cellular origin (YFP fluorescence) or EdU incorporation, or both (Figure 4G and H and Supplementary Figure 11C).

Although this work supports the hypothesis that Schwann cells are a source of GDNF-induced neurons and glia in both myenteric (Figure 4G and H) and submucosal (Supplementary Figure 11C) plexus, it also revealed that



66% of induced neurons were YFP<sup>-</sup>, suggesting a stronger contribution by non-*Dhh*-expressing cell type(s). Regardless of cellular origin, 62% of induced neurons also did not incorporate EdU, raising the possibility that neurogenesis might result from transdifferentiation (ie, direct differentiation of a postmitotic cell into another type of specialized cell) instead of requiring proliferating precursor cells (Figure 4G and H).

### Glial Cell-Derived Neurotrophic Factor Can Induce New Neurons in Human Aganglionic Colon Ex Vivo

To test whether GDNF could induce new enteric neurons in human tissue, we needed an ex vivo model. We discovered that 96 hours of ex vivo GDNF treatment induced neurons in all *Hol<sup>Tg/Tg</sup>* distal colon aganglionic tissues, but neurogenesis was much less efficient than in vivo (Figure 5A and Supplementary Figure 12A). Induced neurons rarely clustered into ganglia, and such ganglia were always very small (Figure 5B). In marked contrast to widespread EdU incorporation into Schwann cells (Figure 5C and Supplementary Figure 12B), EdU incorporation in induced neurons was also minimal (Figure 5B and C).

Although not perfect, we used this ex vivo system to test whether GDNF could induce neurogenesis in aganglionic human colon muscle from children who had pull-through surgery to resect aganglionic distal bowel. Our cohort consisted of 12 children with epidemiologic characteristics typical of HSCR (ie, mostly sporadic, male-biased, s-HSCR) (Table 1). Culturing small pieces of freshly-isolated muscularis externa with GDNF for 96 hours markedly increased the proportion of EdU<sup>+</sup> Schwann cells in 9 of 9 human tissues where EdU was added to media (Figure 5D and E). Most importantly, we also detected new neurons expressing HuC/D,  $\beta$ III-tubulin (Tuj1), RET, PGP9.5, and PHOX2B in 3 HSCR explants (Figure 5F and G; Supplementary Figure 13 and Supplementary Figure Video 4). These 3 explants were from the youngest children of our cohort (28 to 44 days old) (Figure 5G and Table 1). Two of these young children had sporadic HSCR with unknown genetic causes. The third child had a multiple endocrine neoplasia type 2

syndrome-associated *RET* mutation (Table 1). For 2 older children (86 and 1638 days old), we found that extending GDNF treatment to 7 days could yield neurons that incorporated EdU (Figure 5H). Collectively these data suggest our observations in mice may be extended to humans.

## Discussion

Here we report that GDNF enemas can regenerate a functional ENS in situ and prevent death in 3 genetically distinct mouse models of S-HSCR. Detailed mechanistic studies in *Hol<sup>Tg/Tg</sup>* mice showed that exogenous GDNF can penetrate the permeable distal aganglionic colon, leading to increased levels of endogenous GDNF and RET in the whole colon. At least some of the new neurons and glia appear to arise from extrinsic *Dhh-Cre<sup>+</sup>* lineage Schwann cells, and newly organized enteric ganglia appear to be self-sustaining until at least P56 (Supplementary Figure 14).

One concern for GDNF-based therapy is that RET signaling is often reduced in children with HSCR, suggesting GDNF responsiveness would also be reduced. However, most children with S-HSCR must have substantial RET activity in ENS precursors because complete RET absence causes a much more severe phenotype (ie, total intestinal aganglionosis) in mice and humans.<sup>28,34</sup> Supporting this idea, recent whole-genome sequencing studies of people with S-HSCR found only 4.3% (of 443 patients)<sup>7</sup> and 6.3% (of 190 patients)<sup>9</sup> had *RET* rare coding variants predicted to be damaging. Furthermore, rectal GDNF therapy increased levels of RET and endogenous GDNF in mouse colon, suggesting positive feedback loops that could enhance RET signaling even if initial RET levels were low. This could be particularly valuable, because RET provides trophic support to some enteric neurons in adults<sup>4</sup> and is expressed in a subset of GDNF-induced neurons after rectal therapy (Figure 4C and Supplementary Figures 10A and B and 11D).

Finally, although some of the GDNF-induced neurons that express RET are derived from Schwann cells (Supplementary Figure 11D), RET is most likely not needed to activate these precursors in aganglionic bowel. GDNF signaling in Schwann cells is instead mediated by NCAM,<sup>20</sup>

**Figure 3.** Phenotypic and functional characterization of the GDNF-induced ENS in P20 *Hol<sup>Tg/Tg</sup>* mice. (A) WT-like neuron (HuC/D<sup>+</sup>)-to-glia (SOX10<sup>+</sup>) ratio, and (B) proportions of nitrergic and cholinergic neurons in GDNF-induced myenteric ganglia from the distal colon of *Hol<sup>Tg/Tg</sup>* mice (n = 6 mice per group; 3 fields of view per animal). (C) GDNF-induced myenteric ganglia include many neuron subtypes (arrows; n = 3 mice per marker). Scale bar, 20  $\mu$ m. (D) Bead latency test (n = 8–9 mice per group). \**P* < .05; 1-way analysis of variance (ANOVA) with post hoc Sidak's test. (E) Electric field-stimulated and drug-modulated patterns of longitudinal muscle contraction-relaxation (n = 6 WT and *Hol<sup>Tg/Tg</sup>*, n = 7 *Hol<sup>Tg/Tg</sup>* + GDNF). L-NAME, N<sup>G</sup>-nitro-L-arginine methyl ester. \*\**P* < .01; \*\*\*\**P* < .0001; 2-way ANOVA with post hoc Tukey's test. Contractile strength is expressed as the difference from baseline of the area under the curve (AUC) values obtained after stimulation (see Supplementary Figure 6B). Muscle strips from GDNF-treated *Hol<sup>Tg/Tg</sup>* mice are either unresponsive (ie, like untreated *Hol<sup>Tg/Tg</sup>* mice; 3 of 7) or responsive (ie, similar to WT; 4 of 7). (F) Mucosal permeability to FD4 in Ussing's chambers (n = 6 mice per group). \**P* < .05; \*\**P* < .01; 1-way ANOVA with post hoc Sidak's test. (G–I) H&E staining-based analysis of smooth muscle thickness (brackets in G and quantification in H) and neutrophil invasion (asterisks in G and quantification in I) in distal colon sections (n = 6 mice per group) Scale bar, 150  $\mu$ m. \**P* < .05; \*\**P* < .01; \*\*\**P* < .001; 1-way ANOVA with post hoc Sidak's test. (J and K) 16S rRNA sequencing-based microbiome profiling (n = 5 mice per group). (J) Bar histograms display the average relative abundance at the genera level with the SD (error bars). \**P* < .05; 1-way ANOVA with post hoc Tukey's test. (K) Beta diversity comparisons with 95% confidence interval ellipses are based on nonmetric multidimensional scaling (NMDS) of Bray-Curtis dissimilarity of the relative abundance of operational taxonomic units among samples. *P* < .001; permutational multivariate ANOVA.

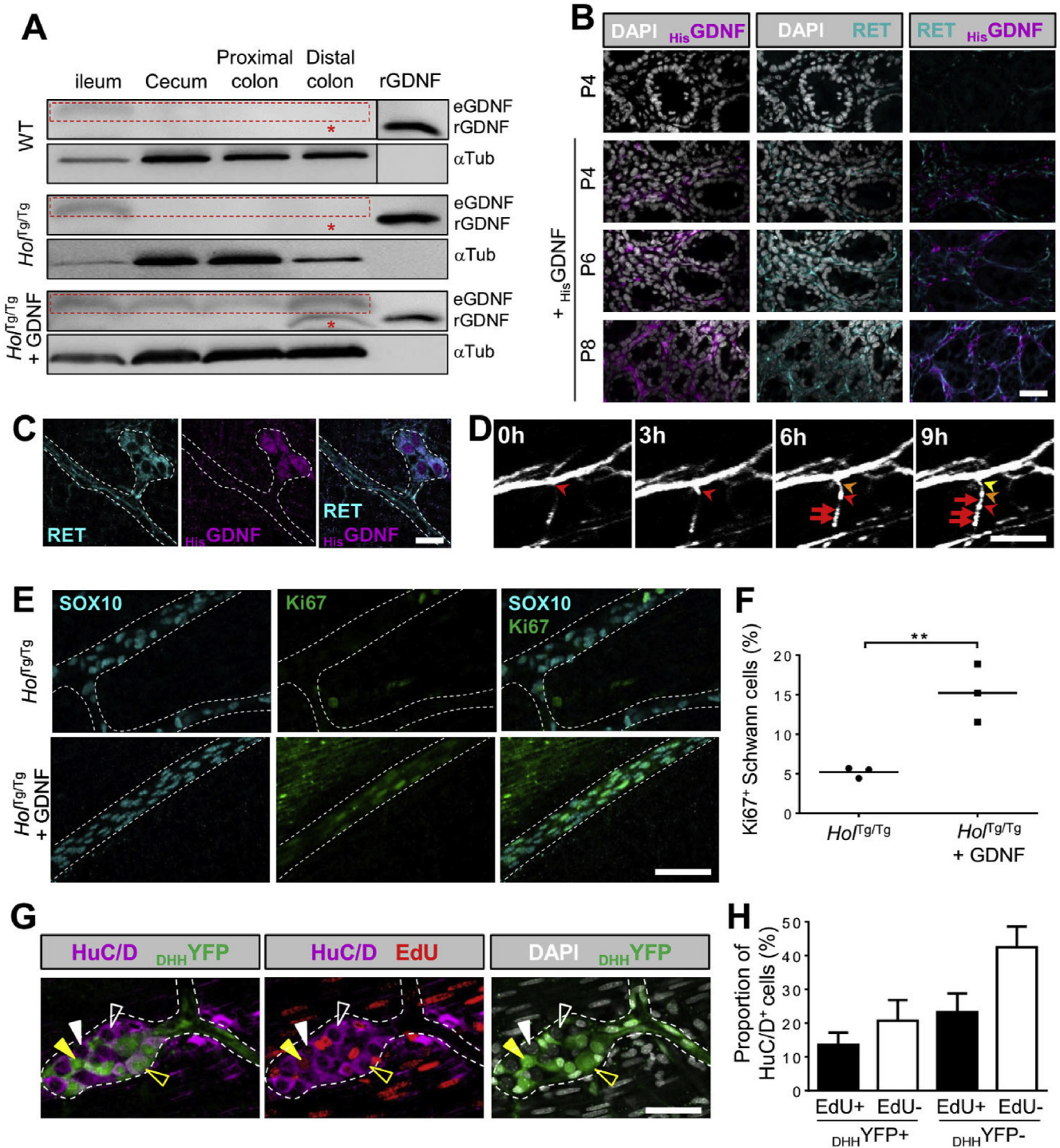


**Figure 4.** Extrinsic Schwann cells are a source of GDNF-induced neurons and glia in the otherwise aganglionic colon. (A) Distribution of recombinant (r)GDNF (asterisks) and endogenous (e)GDNF (dashed boxes) in different subregions of the gastrointestinal tract from WT,  $Ho1^{Tg/Tg}$ , and GDNF-treated  $Ho1^{Tg/Tg}$  mice at P8.  $\alpha$ -Tub,  $\alpha$ -tubulin. Accumulation of 6XHis-tagged GDNF ( $_{His}$ GDNF) and RET during enema treatments of  $Ho1^{Tg/Tg}$  mice (B) in the submucosa between P4 and P8 and (C) in induced myenteric neurons at P8. (D) Ten-hour-long time-lapse recordings of GDNF-cultured aganglionic colon tissues from P4  $Ho1^{Tg/Tg};G4-RFP$  mice showing GDNF-induced Schwann cells dividing (arrows) and migrating (arrowheads) on extrinsic nerves (50- $\mu$ m-thick z-stacks). (E and F) GDNF exposure for 96 hours increases Schwann cell proliferation (SOX10<sup>+</sup> Ki67<sup>+</sup>) in distal colon explants from P4  $Ho1^{Tg/Tg}$  mice. **\*\*** $P < .01$ ; 2-tailed Student's  $t$  test. (G and H) Myenteric ganglia from the distal colon of P20  $Ho1^{Tg/Tg};Dhh-Cre^{Tg/+};R26^{YFP/+}$  mice that were administered GDNF and EdU between P4 and P8. Data are presented with the SD (error bars). Four categories of induced neuron are detected: (1) EdU<sup>+</sup> Schwann-derived (filled yellow arrowhead); (2) EdU<sup>-</sup> Schwann-derived (empty yellow arrowhead); (3) EdU<sup>+</sup> unknown origin (filled white arrowhead); and (4) EdU<sup>-</sup> unknown origin (empty white arrowhead). All blots/images are representative of observations made from 3 mice. Quantifications were performed using 3 fields of view per mouse. The dashed outlines delineate (E) either an extrinsic nerve fiber, or (C and G) an extrinsic nerve fiber and an adjacent single ganglion. Scale bar, 20  $\mu$ m (B and C), 100  $\mu$ m (D), 50  $\mu$ m (E and F).

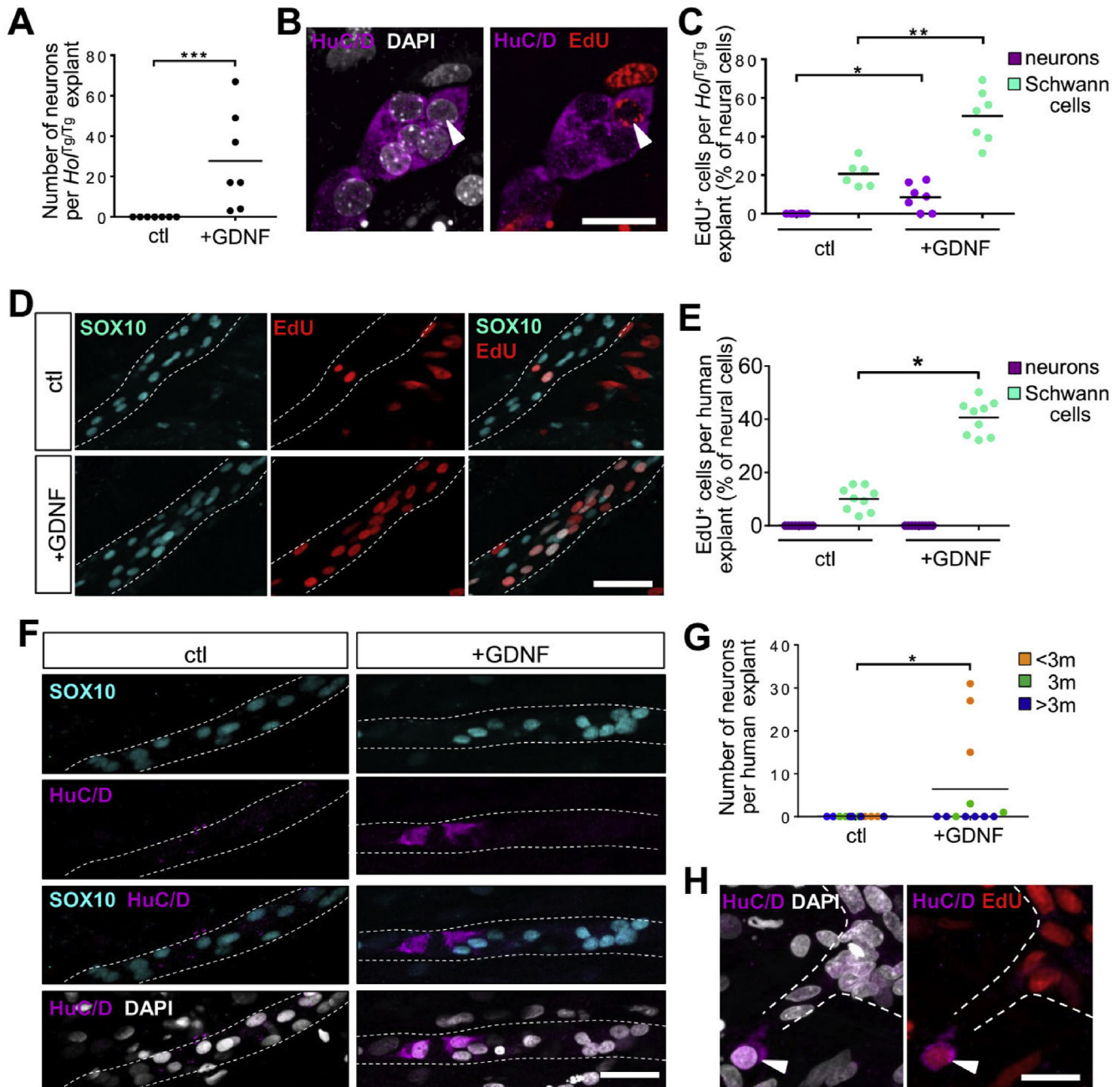


**Figure 5.** Ex vivo preclinical testing of GDNF therapy on explants of aganglionic colon from *Ho1<sup>Tg/Tg</sup>* mice and HSCR patients. (A–C) Distal colon explants from P4 *Ho1<sup>Tg/Tg</sup>* mice cultured for 96 hours with GDNF and EdU (+GDNF) or EdU alone (ctl). (A) GDNF-induced *HuC/D*<sup>+</sup> neurons rarely form ganglia and (B) are less likely to show EdU incorporation than *SOX10*<sup>+</sup> Schwann cells (arrowhead in B and quantification in C) ( $n = 7$  explants per condition). \* $P < .05$ ; \*\* $P < .01$ ; \*\*\* $P < .001$ ; 2-tailed Mann-Whitney *U* test. (D–G) Aganglionic colon explants from human HSCR patients cultured for 96 hours with GDNF and EdU (+GDNF) or EdU alone (ctl). (D and E) EdU incorporation was detected in *SOX10*<sup>+</sup> Schwann cells but not in *HuC/D*<sup>+</sup> neurons. (F) GDNF-induced *HuC/D*<sup>+</sup> neurons were detected in a subset of explants, (G) all originating from patients less than 3 months of age at the time of surgery ( $n = 12$  explants per condition). \* $P < .05$ ; 2-tailed Mann-Whitney *U* test. (H) Extended culture in the presence of GDNF for 7 days yielded neurons in explants from older patients, including some that incorporated EdU (arrowhead). All displayed images were taken at the myenteric plexus level. The dashed outlines delineate extrinsic nerve fibers. Scale bars, 50  $\mu\text{m}$  (B and H) and 100  $\mu\text{m}$  (D and F).

and our data show NCAM but not RET expression in Schwann cells of extrinsic nerves in aganglionic mouse colon (Supplementary Figure 15). Nonetheless, we tried to directly determine whether reduced RET levels affected

GDNF therapy using our previously published model of *Ret* hypomorphic mice exposed to mycophenolate.<sup>22</sup> However, several problems complicated interpretation in our new experimental conditions, including the occurrence of

**Table 1.** Overview of Hirschsprung's Disease Colon Samples Used for Ex Vivo Preclinical Testing of Glial Cell-Derived Neurotrophic Factor Therapy

Age at surgery, <i>d</i>	Genetic status	Sex	Clinical classification	Extent of aganglionosis, <i>cm</i>	Neurons, EdU <sup>+</sup> Schwann's cells, %	
28	Sporadic, unknown mutation	M	Short-segment disease	5	31	38
36	Sporadic, unknown mutation	M	Short-segment disease	25	27	33
44	MEN2a syndrome, RET mutation	M	Short-segment disease	6	15	44
80	Sporadic, unknown mutation	M	Short-segment disease	7	3	34
85	Sporadic, unknown mutation	M	Short-segment disease	6	1	32
86	Sporadic, unknown mutation	M	Short-segment disease	7	0	46
249	Mowat-Wilson syndrome, ZFX1B mutation	F	Short-segment disease	30	0	32
300	Data not available	M	Data not available	Data not available	0	Not quantified
344	Sporadic, unknown mutation	M	Short-segment disease	26	0	Not quantified
349	Sporadic, unknown mutation	M	Short-segment disease	9	0	43
1177	Bardet-Biedl syndrome, BBS1 mutation	F	Long-segment disease	40	0	Not quantified
1638	Sporadic, unknown mutation	F	Short-segment disease	8	0	50

F, female; M, male; No., number.

HSCR-like dilated bowel even in absence of aganglionosis (Supplementary Figure 2C and D). Future studies would need to test GDNF enema effects in other models where reduced RET activity is associated with short-segment aganglionosis, but the “ideal” model is not readily apparent.

In contrast to *Ret* mutants, *Hol<sup>Tg/Tg</sup>*, *Tash<sup>Tg/Tg</sup>*, and *Ednrb<sup>s-l/s-l</sup>* mice are all reliable models of S-HSCR,<sup>25–27</sup> recapitulating key hallmarks of the human disease in the aganglionic segment and proximal ENS-containing colonic regions.<sup>29–32</sup> Although not all GDNF-treated mutant mice have prolonged survival, the survival advantage after GDNF treatment in Montreal is dramatic, and the in situ generation of new enteric neurons in previously aganglionic bowel, which was observed in both Montreal and Philadelphia (Supplementary Figure 10A and B), is unprecedented. The reason some mice responded better to GDNF than others might be due to the degree of aganglionosis-associated inflammation (Figure 3G and I). Indeed, although GDNF is known to have anti-inflammatory properties,<sup>35</sup> the inflammatory microenvironment present in aganglionic bowel before GDNF treatment might help trigger a neurogenic response as it does in the context of inflammatory bowel disease.<sup>36</sup> Unfortunately, the exact inflammatory mediators that enhance enteric neurogenesis are not yet known, but once identified, we could develop adjunct treatments that enhance the effect of GDNF therapy.

Adjunct treatments might also be developed based on a serendipitous finding we made when we tried to replicate our Montreal survival data (Figure 1A–C) using *Hol<sup>Tg/Tg</sup>* and *Ednrb<sup>s-l/s-l</sup>* mice in Philadelphia. We unexpectedly discovered that these mouse lines live much longer in Philadelphia than in Montreal without any specific treatment, even though all of our mice originated from the same colonies

(Supplementary Figure 10C and D). The prolonged survival in Philadelphia compared with Montreal was especially dramatic for untreated *Ednrb<sup>s-l/s-l</sup>* (Supplementary Figure 10C), which lived much longer than previously described in any other mouse facility.<sup>27,30,37</sup> Intriguingly, the survival advantage for untreated HSCR models in Philadelphia occurred despite the confirmed presence of distal bowel aganglionosis or megacolon, or both (Supplementary Figure 10C and D). In fact, Philadelphia-based untreated mice survived as long as GDNF-treated mice in Montreal (Supplementary Figure 10E and F), and survival could not be further enhanced in Philadelphia by GDNF treatment (Supplementary Figure 10E and F) even though GDNF-induced neurogenesis was similar in both Montreal and Philadelphia (Supplementary Figure 10A and B). One especially attractive hypothesis for all of these observations is that GDNF treatment in Montreal and nongenetic factors in Philadelphia might both improve a critical prosurvival bowel function (eg, promoting enhanced epithelial barrier function or modulating mucosal immune responses), either indirectly (via induced ENS ganglia) in Montreal or directly (bypassing the need for induced ENS ganglia) in Philadelphia. Although we suspect that food- or microbiota-based mechanisms, or both, underlie the survival advantage in Philadelphia, there are many variables, so defining mechanisms is complicated.

A potentially more straightforward approach to improve GDNF therapy would be to identify GDNF-targeted ENS progenitors other than *Dhh*-lineage Schwann cells that appear to contribute only approximately one-third of GDNF-induced neurons. This could lead to an improved GDNF-based cocktail that includes additional trophic factor(s) that bind receptors on these other cells. In this regard,

substantial literature suggests the existence of ENS “stem cells” in postnatal mouse and human bowel,<sup>38,39</sup> even in aganglionic regions.<sup>40,41</sup> Interestingly, extrinsic nerve fibers of aganglionic regions were previously identified as a niche for these ENS stem cells.<sup>41</sup>

Our data confirm this prior observation and further suggest that at least some of these stem cells are in fact *Dhh*-lineage Schwann cells. It is possible that the other ENS progenitors are also Schwann cells that do not express CRE in *Dhh-Cre* mice. In accordance with this possibility, we noted that some SOX10<sup>+</sup> Schwann cells are not YFP<sup>+</sup> in extrinsic nerves from the aganglionic colon of *Hol<sup>Tg/Tg</sup>;Dhh-Cre<sup>Tg/+</sup>;R26<sup>YFP/+</sup>* mice at P8 (Supplementary Figure 16). The strong contribution of non-*Dhh*-expressing cells combined with the location of some GDNF-induced ganglia away from extrinsic nerves, however, also suggests the involvement of additional cell type(s), which might include sacral neural crest-derived cells. Sacral-derived ENS progenitors can colonize the aganglionic colon during prenatal development,<sup>42</sup> and our SOX10 immunofluorescence data suggest that some of these cells persist in postnatal aganglionic tissues as scattered progenitors or enteric glia, or both, also expressing the alternative GDNF receptor neural cell adhesion molecule (Figure 2A and Supplementary Figure 15). A contribution by differentiated enteric glia of sacral origin might also help explain the observation that many GDNF-induced neurons had not incorporated EdU, suggesting they were generated via transdifferentiation (Figure 4G and H).

In theory, GDNF-based rectal therapy would be easy to implement because normal saline enemas are already commonly used in children with HSCR before and after pull-through surgery. If penetration of GDNF beyond the epithelium was limited, GDNF could be directly injected into the colon wall with currently available endoscopes or via a specially designed delivery tool. Ideally, GDNF-based rectal therapy would prevent the need for pull-through surgery. Even if GDNF enemas did not work as primary HSCR treatment, GDNF therapy might nevertheless improve postsurgical outcomes by normalizing ENS structure in the retained distal bowel of the “transition zone” (ie, correcting hypoganglionosis and neuronal subtype imbalance). In addition, because ENS stem cell-based therapies are being considered for the treatment of HSCR, GDNF might be a useful adjunct to these therapies to promote engraftment. All of these considerations make a human clinical trial of GDNF-based rectal therapy in children with HSCR appealing.

## Supplementary Material

Note: To access the supplementary material accompanying this article, visit the online version of *Gastroenterology* at [www.gastrojournal.org](http://www.gastrojournal.org), and at <https://doi.org/10.1053/j.gastro.2020.07.018>.

## References

1. Furness JB. The enteric nervous system and neurogastroenterology. *Nat Rev Gastroenterol Hepatol* 2012; 9:286–294.
2. Heuckeroth RO. Hirschsprung disease-integrating basic science and clinical medicine to improve outcomes. *Nat Rev Gastroenterol Hepatol* 2018;15:152–167.
3. Heuckeroth RO, Schafer KH. Gene-environment interactions and the enteric nervous system: Neural plasticity and Hirschsprung disease prevention. *Dev Biol* 2016;417:188–197.
4. Gianino S, Grider JR, Cresswell J, et al. GDNF availability determines enteric neuron number by controlling precursor proliferation. *Development* 2003;130:2187–2198.
5. Natarajan D, Marcos-Gutierrez C, Pachnis V, et al. Requirement of signalling by receptor tyrosine kinase RET for the directed migration of enteric nervous system progenitor cells during mammalian embryogenesis. *Development* 2002;129:5151–5160.
6. Young HM, Hearn CJ, Farlie PG, et al. GDNF is a chemoattractant for enteric neural cells. *Dev Biol* 2001; 229:503–516.
7. Tang CS, Li P, Lai FP, et al. Identification of genes associated with Hirschsprung disease, based on whole-genome sequence analysis, and potential effects on enteric nervous system development. *Gastroenterology* 2018;155:1908–1922 e5.
8. Emison ES, Garcia-Barcelo M, Grice EA, et al. Differential contributions of rare and common, coding and non-coding Ret mutations to multifactorial Hirschsprung disease liability. *Am J Hum Genet* 2010;87:60–74.
9. Tilghman JM, Ling AY, Turner TN, et al. Molecular genetic anatomy and risk profile of Hirschsprung’s disease. *N Engl J Med* 2019;380:1421–1432.
10. Gui H, Schriemer D, Cheng WW, et al. Whole exome sequencing coupled with unbiased functional analysis reveals new Hirschsprung disease genes. *Genome Biol* 2017;18:48.
11. Tang CS, Zhuang X, Lam WY, et al. Uncovering the genetic lesions underlying the most severe form of Hirschsprung disease by whole-genome sequencing. *Eur J Hum Genet* 2018;26:818–826.
12. Swenson O, Bill AH Jr. Resection of rectum and rectosigmoid with preservation of the sphincter for benign spastic lesions producing megacolon; an experimental study. *Surgery* 1948;24:212–220.
13. Burns AJ, Goldstein AM, Newgreen DF, et al. White paper on guidelines concerning enteric nervous system stem cell therapy for enteric neuropathies. *Dev Biol* 2016; 417:229–251.
14. McCann CJ, Borrelli O, Thapar N. Stem cell therapy in severe pediatric motility disorders. *Curr Opin Pharmacol* 2018;43:145–149.
15. Yntema CL, Hammond WS. The origin of intrinsic ganglia of trunk viscera from vagal neural crest in the chick embryo. *J Comp Neurol* 1954;101:515–541.
16. Hotta R, Anderson RB, Kobayashi K, et al. Effects of tissue age, presence of neurones and endothelin-3 on the ability of enteric neurone precursors to colonize recipient gut: implications for cell-based therapies. *Neurogastroenterol Motil* 2010;22. 331–e86.
17. Le Douarin NM, Teillet MA. The migration of neural crest cells to the wall of the digestive tract in avian embryo. *J Embryol Exp Morphol* 1973;30:31–48.

18. Uesaka T, Nagashimada M, Enomoto H. Neuronal differentiation in Schwann cell lineage underlies postnatal neurogenesis in the enteric nervous system. *J Neurosci* 2015;35:9879–9888.
19. Watanabe Y, Ito F, Ando H, et al. Morphological investigation of the enteric nervous system in Hirschsprung's disease and hypoganglionosis using whole-mount colon preparation. *J Pediatr Surg* 1999;34:445–449.
20. Paratcha G, Ledda F, Ibanez CF. The neural cell adhesion molecule NCAM is an alternative signaling receptor for GDNF family ligands. *Cell* 2003;113:867–879.
21. Sjostrand D, Ibanez CF. Insights into GFRalpha1 regulation of neural cell adhesion molecule (NCAM) function from structure-function analysis of the NCAM/GFRalpha1 receptor complex. *J Biol Chem* 2008;283:13792–13798.
22. Lake JI, Tusheva OA, Graham BL, et al. Hirschsprung-like disease is exacerbated by reduced de novo GMP synthesis. *J Clin Invest* 2013;123:4875–4887.
23. **Creedon DJ, Tansey MG**, Baloh RH, et al. Neurturin shares receptors and signal transduction pathways with glial cell line-derived neurotrophic factor in sympathetic neurons. *Proc Natl Acad Sci U S A* 1997;94:7018–7023.
24. Toure AM, Landry M, Souchkova O, et al. Gut microbiota-mediated gene-environment interaction in the TashT mouse model of Hirschsprung disease. *Sci Rep* 2019;9:492.
25. Soret R, Mennetrey M, Bergeron KF, et al. A collagen VI-dependent pathogenic mechanism for Hirschsprung's disease. *J Clin Invest* 2015;125:4483–4496.
26. **Bergeron KF, Cardinal T**, Toure AM, et al. Male-biased aganglionic megacolon in the TashT mouse line due to perturbation of silencer elements in a large gene desert of chromosome 10. *PLoS Genet* 2015;11:e1005093.
27. Hosoda K, Hammer RE, Richardson JA, et al. Targeted and natural (piebald-lethal) mutations of endothelin-B receptor gene produce megacolon associated with spotted coat color in mice. *Cell* 1994;79:1267–1276.
28. Schuchardt A, D'Agati V, Larsson-Blomberg L, et al. Defects in the kidney and enteric nervous system of mice lacking the tyrosine kinase receptor Ret. *Nature* 1994;367:380–383.
29. Cheng LS, Schwartz DM, Hotta R, et al. Bowel dysfunction following pullthrough surgery is associated with an overabundance of nitrergic neurons in Hirschsprung disease. *J Pediatr Surg* 2016;51:1834–1838.
30. **Ro S, Hwang SJ**, Muto M, et al. Anatomic modifications in the enteric nervous system of piebald mice and physiological consequences to colonic motor activity. *Am J Physiol Gastrointest Liver Physiol* 2006;290:G710–G718.
31. Toure AM, Charrier B, Pilon N. Male-specific colon motility dysfunction in the TashT mouse line. *Neurogastroenterol Motil* 2016;28:1494–1507.
32. **Zaitoun I, Erickson CS**, Barlow AJ, et al. Altered neuronal density and neurotransmitter expression in the ganglionated region of Ednrb null mice: implications for Hirschsprung's disease. *Neurogastroenterol Motil* 2013;25:e233–e244.
33. Pilon N, Raiwet D, Viger RS, et al. Novel pre- and post-gastrulation expression of Gata4 within cells of the inner cell mass and migratory neural crest cells. *Dev Dyn* 2008;237:1133–1143.
34. Shimotake T, Go S, Inoue K, et al. A homozygous missense mutation in the tyrosine E kinase domain of the RET proto-oncogene in an infant with total intestinal aganglionosis. *Am J Gastroenterol* 2001;96:1286–1291.
35. Zhang DK, He FQ, Li TK, et al. Glial-derived neurotrophic factor regulates intestinal epithelial barrier function and inflammation and is therapeutic for murine colitis. *J Pathol* 2010;222:213–222.
36. Belkind-Gerson J, Hotta R, Nagy N, et al. Colitis induces enteric neurogenesis through a 5-HT4-dependent mechanism. *Inflamm Bowel Dis* 2015;21:870–878.
37. Fujimoto T. Natural history and pathophysiology of enterocolitis in the piebald lethal mouse model of Hirschsprung's disease. *J Pediatr Surg* 1988;23:237–242.
38. Kruger GM, Mosher JT, Bixby S, et al. Neural crest stem cells persist in the adult gut but undergo changes in self-renewal, neuronal subtype potential, and factor responsiveness. *Neuron* 2002;35:657–669.
39. Laranjeira C, Sandgren K, Kessaris N, et al. Glial cells in the mouse enteric nervous system can undergo neurogenesis in response to injury. *J Clin Invest* 2011;121:3412–3424.
40. Badizadegan K, Thomas AR, Nagy N, et al. Presence of intramucosal neuroglial cells in normal and aganglionic human colon. *Am J Physiol Gastrointest Liver Physiol* 2014;307:G1002–G1012.
41. Wilkinson DJ, Bethell GS, Shukla R, et al. Isolation of enteric nervous system progenitor cells from the aganglionic gut of patients with Hirschsprung's disease. *PLoS One* 2015;10:e0125724.
42. Burns AJ, Champeval D, Le Douarin NM. Sacral neural crest cells colonise aganglionic hindgut in vivo but fail to compensate for lack of enteric ganglia. *Dev Biol* 2000;219:30–43.

---

Author names in bold designate shared co-first authorship.

Received April 22, 2020. Accepted July 10, 2020.

#### Correspondence

Address correspondence to: Nicolas Pilon, Département des Sciences Biologiques, Université du Québec à Montréal (UQAM), 141 Président-Kennedy Avenue, Montréal, Québec H2X 3Y7, Canada. e-mail: pilon.nicolas@uqam.ca.

#### Acknowledgments

GB is presently affiliated with Plateforme de transgénèse, Centre de recherche du centre hospitalier de l'Université de Montréal, Montréal, Québec, Canada.

FR-G is presently affiliated with the Division of Pediatric Gastroenterology, Hepatology and Nutrition, Children's Hospital, Lucerne, Switzerland.

The authors thank Denis Fiipo (Université du Québec à Montréal) for assistance with confocal imaging, Dr Natalie Patey (Centre hospitalier universitaire Ste-Justine), Ben Wilkins and Archana Shenoy (Children's Hospital of Philadelphia) for help with collection of human samples, and MedGenesis Therapeutics Inc for generously providing clinical-grade human recombinant glial cell-derived neurotrophic factor.

#### CRedit Authorship Contributions

Rodolphe Soret, PhD (Conceptualization: Supporting; Data curation: Lead; Formal analysis: Lead; Investigation: Lead; Methodology: Lead; Writing –

original draft: Supporting; Writing – review & editing: Supporting). Sabine Schneider, BSc (Data curation: Supporting; Formal analysis: Supporting; Investigation: Supporting; Writing – review & editing: Supporting). Guillaume Bernas, MSc (Formal analysis: Supporting; Investigation: Supporting). Briana Christophers, BSc (Formal analysis: Supporting). Ouliana Souchkova, MSc (Formal analysis: Supporting). Baptiste Charrier, MSc (Formal analysis: Supporting). Franziska Righini-Grunder, MD, MSc (Resources: Equal). Ann Aspirot, MD (Resources: Equal). Mathieu Landry, MSc (Data curation: Supporting; Formal analysis: Supporting). Steven W. Kembel, PhD (Data curation: Supporting). Christophe Faure, MD (Resources: Supporting). Robert O. Heuckeroth, MD, PhD (Funding acquisition: Supporting; Supervision: Supporting; Writing – original draft: Equal; Writing – review & editing: Equal). Nicolas Pilon, PhD (Conceptualization: Lead; Funding acquisition: Lead; Project administration: Lead; Supervision: Lead; Writing – original draft: Lead; Writing – review & editing: Lead).

**Conflicts of interest**

The authors disclose no conflicts.

**Funding**

This work was supported by catalyst grants from the Fondation du grand défi Pierre Lavoie to N.P. and by an operating grant from the Canadian Institutes of Health Research (CIHR #377028) to N.P. and R.O.H. R.S. was supported by a postdoctoral fellowship from the Fonds de la recherche du Québec—Santé (FRQS). S.W.K. holds the Canada Research Chair in Plant Microbiomes. N.P. is a FRQS Senior Research Scholar and the recipient of the UQAM Research Chair on Rare Genetic Diseases. R.O.H. was also supported by the March of Dimes 6-FY15-235, the Irma and Norman Braman Endowment, the Suzi and Scott Lustgarten Center Endowment, and the Children's Hospital of Philadelphia Research Institute. The funders had no role in study design, data collection and analysis, decision to publish, or preparation of the manuscript.

## Supplementary Methods

### Mice

*Holstein* (*Tg[Sox3-GFP,Tyr]HolNpln*), *TashT* (*Tg[SRY-YFP,Tyr]TashTNpln*), and *G4-RFP* (*Gata4p[5kb]-RFP*) lines were as previously described (all maintained on a FVB/N genetic background),<sup>1-3</sup> whereas *Piebald-lethal* (*Ednrb<sup>sl</sup>*; JAX stock #000308; C3H/HeJ-C57BL/6 mixed background) and *Dhh-Cre* (*Tg[Dhh-cre]1Mejr*; JAX stock #012929; FVB/N background) were obtained from The Jackson Laboratory (Bar Harbor, ME). Other mouse lines used were *R26<sup>Floxed Stop</sup>YFP* (*Gt[ROSA]26Sor<sup>tm1(EYFP)Cos</sup>*, provided by F. Costantini (Columbia University, New York, NY), and maintained on a FVB/N background),<sup>4</sup> *Ret<sup>TGM</sup>* (here referred to as *Ret*-null; *Ret<sup>tm1Jmi</sup>*; maintained on a C57BL/6 background),<sup>5</sup> and *Ret<sup>9</sup>* (*Ret<sup>tm2(RET)Jmi</sup>*, provided by S. Jain (Washington University in St. Louis School of Medicine, St. Louis, MO), and maintained on a 129X1/Sv1 background).<sup>6</sup>

For mycophenolate mofetil treatments,<sup>7</sup> timed pregnancies were set up by mating *Ret<sup>+/-</sup>* with *Ret<sup>9/+</sup>* or *Ret<sup>9/9</sup>* mice, considering noon of the day of plug detection as E0.5. At E7.5, the drinking water of pregnant dams was replaced with 0.25X PBS adjusted to pH 3.6 with added prodrug mycophenolate mofetil (NDC Cat. #16729-094, Accord Healthcare, Durham, NC) at concentrations of 250  $\mu\text{g/mL}$ , 187.5  $\mu\text{g/mL}$ , and 125  $\mu\text{g/mL}$ . Dams remained on mycophenolate mofetil-supplemented drinking water from E7.5 to E18.5.

GDNF enemas were administered using a 24-gauge gavage needle (Fine Science Tools, Vancouver, BC, Canada) attached to a micropipette. The head of the gavage needle was introduced in the rectum just beyond the anus, and enemas were injected over the course of a few seconds. Pups were then placed back with their mother and either sacrificed for tissue analysis (at the age indicated in relevant figure legends) or checked daily to track survival. Apart from GDNF, other tested molecules (each at 10  $\mu\text{g}$  in 10  $\mu\text{L}$  PBS) included the serotonin receptor (5-hydroxytryptamine receptor 4) agonist RS67506 (Cat. #0990, R&D Systems, Minneapolis, MN), Noggin (Cat. #SRP4675; Sigma-Aldrich, St Louis, MO), endothelin-3 (Cat. #E9137; Sigma-Aldrich), serotonin (Cat. #H9523; Sigma-Aldrich), and L-ascorbic acid (Cat. # A4403; Sigma-Aldrich) (rationale provided in [Supplementary Table 1](#)).

### Tissue Labeling and Imaging

For immunofluorescence staining, whole microdissected tissues were permeabilized for 2 hours in blocking solution (10% fetal bovine serum and 1% Triton X-100, in PBS) before being sequentially incubated with specific primary (at 4°C overnight) and relevant secondary (at room temperature for 2 hours) antibodies, with both diluted in blocking solution that was also used to wash tissues between all steps. All antibodies and dilution factors are listed in [Supplementary Table 2](#). EdU was detected using the Invitrogen Click-iT EdU Imaging Kit (Cat. #C10337; Thermo Fisher Scientific) in accordance with the manufacturer's instructions. For histologic analyses, cross-sections of full-

thickness bowel tissues were stained with H&E, as previously described.<sup>8</sup>

All immunofluorescence images were acquired with a 20 $\times$  or a 60 $\times$  objective on a confocal microscope (Nikon A1R [Melville, NY] or Zeiss 710 [Thornwood, NY]), with the exception of H&E-stained sections, which were imaged with a 10 $\times$  objective using an Infinity-2 camera (Lumenera Corp, Ottawa, ON, Canada) mounted on a Leica DM 2000 microscope (Leica Microsystems, Richmond Hill, ON, Canada). Image analysis was performed with ImageJ (National Institutes of Health, Bethesda, MD), using the "Subtract background" function to decrease nonspecific background signal, the "Multi-point" function for cell counting, and the "Polygon selection" function for calculation of surface area.

### Western Blot Analysis

Organs dissolved in radioimmunoprecipitation assay buffer (containing 1X Complete Protease Inhibitors; Roche, Indianapolis, IN) were sonicated on ice and centrifuged at 14,000 rpm for 15 minutes at 4°C, keeping the supernatants for Western blot analysis. Equal volumes of samples were electrophoretically separated in an 18% sodium dodecyl sulfate-polyacrylamide gel and transferred to Immobilon-P nitrocellulose membranes (Cat. #1620177, Bio-Rad, Hercules, CA). Membranes were subsequently incubated in blocking solution (5% skimmed milk and 0.1% Tween 20, in Tris-buffered saline), followed by incubation with mouse anti-GDNF (1:500 dilution factor; Cat. #sc-13147; Santa Cruz Biotechnology, Dallas, TX) or rabbit anti- $\alpha$ -tubulin (1:70 000 dilution factor; Cat. #ab176560; Abcam, Cambridge, MA) primary antibodies, and then relevant horseradish peroxidase-conjugated secondary antibodies, all diluted in blocking solution. Each incubation was for 60 minutes at room temperature, each time interspersed by 3 washes with blocking solution. Proteins were finally visualized using Immobilon Western Chemiluminescent HRP Substrate (Cat. #WBKLS0050, MilliporeSigma, Burlington, MA) and Fusion FX imaging system (Vilber, Marne-la-Vallée, France).

### Ex Vivo Culture for Time-Lapse Imaging

Muscle strips were cultured in suspension as previously described for time-lapse imaging of embryonic guts<sup>3</sup> in Dulbecco's Modified Eagles Medium/F12 medium (Cat. #319-085-CL; WISENT, St-Bruno, QC, Canada) supplemented with 10% fetal bovine serum and 100 IU/mL antibiotic-antimycotic, with or without, 5  $\mu\text{g/mL}$  GDNF under standard culture conditions (37°C, 5% CO<sub>2</sub>). After 72 hours of culture, each Petri dish was placed in a microscope incubation chamber (Okolab USA, Ambridge, PA) for 10 hours under the same culture conditions, and image stacks (250  $\mu\text{m}$  thick) of RFP-labeled extrinsic nerves and Schwann cells were acquired every 10 minutes, using a 20 $\times$  objective on a Nikon A1R confocal unit, as previously described.<sup>3</sup>

### In Vivo and Ex Vivo Analysis of Colonic Motility

For the bead latency test, mice were anesthetized with 2% isoflurane, and a 2-mm glass bead (Cat. #1.04014,

Sigma-Aldrich) was inserted into the distal colon with a probe over a distance of 0.5 cm from the anus. Each mouse was then isolated in its cage without access to food and water, and monitored for the time required to expel the glass bead.

For *ex vivo* analysis of contractility, muscle strips were initially stretched with a preload of 2 g of tension for 60 minutes, and contraction/relaxation of longitudinal muscles was then continuously recorded with a myograph (Model F-60; Narco Biosystems Inc, Houston, TX) coupled to a computer equipped with the BIOPAC student Lab 4.0.2 software (BIOPAC Systems Inc, Goleta, CA). Electrical field stimulation (EFS) was applied with a voltage stimulator (Model BSL MP36/35, BIOPAC Systems Inc) connected to electrodes, using parameters that activate enteric neurons without directly activating muscles (12 V, 20 Hz, 10-second train duration, and 300  $\mu$ s stimulus pulse duration). This procedure was repeated 3 times, with 10-minute washout periods between stimulations.

To characterize the nitrergic and cholinergic components of EFS-induced contractile responses,  $N^G$ -nitro-L-arginine methyl ester (L-NAME; Cat. #N5751; Sigma-Aldrich) and atropine (Cat. #A01132; Sigma-Aldrich) were added to Krebs solution at a final concentration of 0.5  $\mu$ mol/L and 1  $\mu$ mol/L, respectively. The area under the curve (AUC) was measured during each EFS-induced response, and data were expressed in  $\Delta$ AUC (corresponding to the difference between the AUC measured 20 seconds after stimulation minus the AUC measured 20 seconds before stimulation).

### Ex Vivo Analysis of Paracellular Permeability

Each Ussing chamber contained 5 mL of Dulbecco's modified Eagle medium/F12 medium (Cat. #319-085-CL; Wisent), which was maintained at 37°C and continuously oxygenated (95% O<sub>2</sub>/5% CO<sub>2</sub>). After a 30-minute equilibration period, 200  $\mu$ L of apical medium was replaced with 200  $\mu$ L of a 1 mg/mL solution of fluorescein isothiocyanate-conjugated dextran, 4 kDa (FD4; Cat. #60842-46-8; Sigma-Aldrich). Fluorescence intensity of basolateral aliquots of 150  $\mu$ L, reflecting paracellular transit from the luminal surface, was then measured every 30 minutes over a period of 3 hours, using a fluorimeter (Model Infinite M1000, Tecan, Männedorf, Switzerland). Fluorescence intensity was finally converted in amount of FD4 by comparison with a standard curve, and the average value for the 3-hour period was used to calculate paracellular permeability, which was expressed in nanograms of FD4 per surface of mucosa area per minute ( $\text{ng} \cdot \text{cm}^{-2} \cdot \text{min}^{-1}$ ).

### Microbiome Analysis

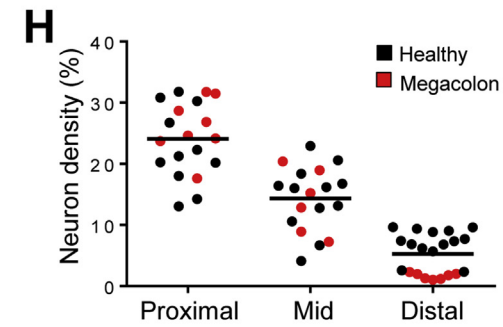
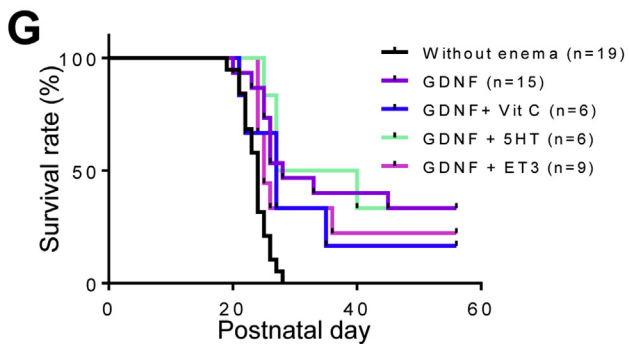
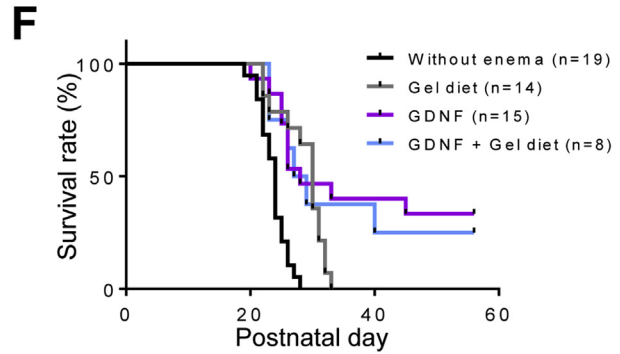
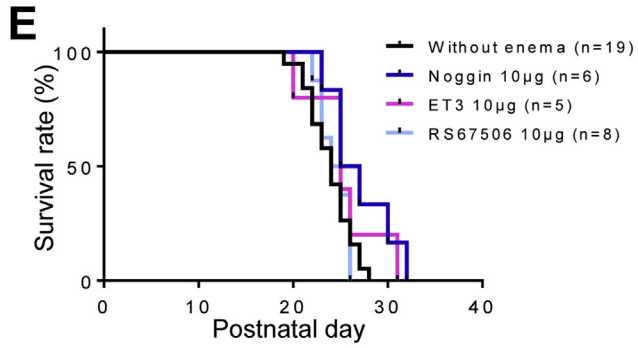
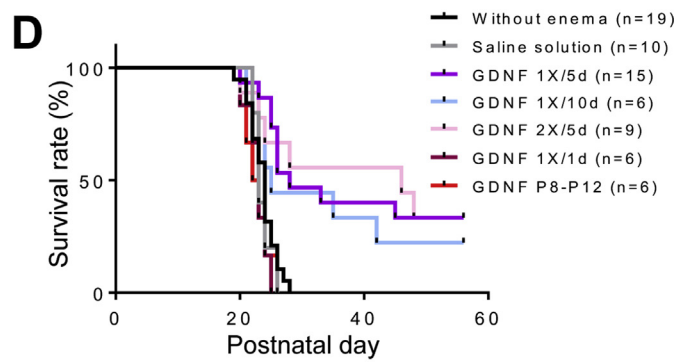
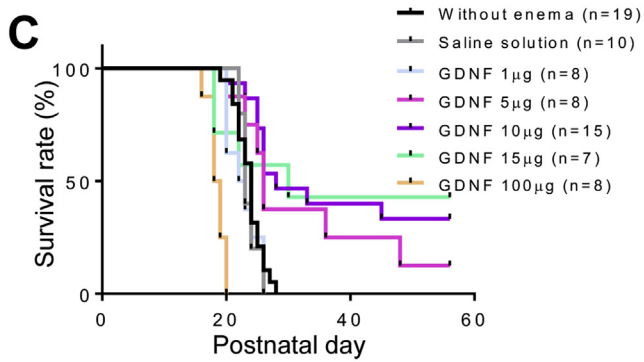
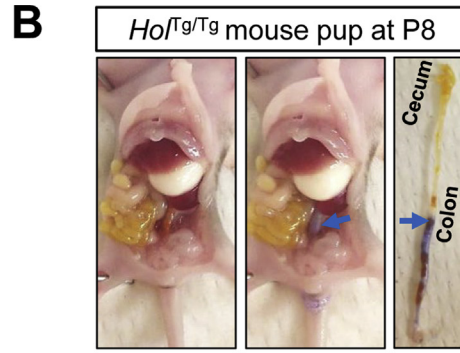
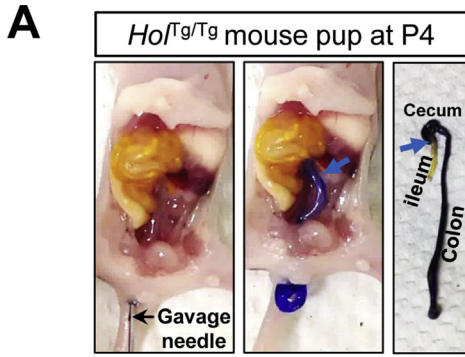
Mice were sacrificed at P20, and 3 fecal pellets per mouse were directly collected from the colon. Bacterial DNA was then extracted using the QIAamp Fast DNA Stool Mini Kit (Cat. # 51604; QIAGEN, Valencia, CA), and the V5-V6 region of the 16S rRNA gene was amplified with polymerase chain reaction with a collection of previously described bar-coded primers.<sup>9</sup> Raw sequences generated with an MiSeq

sequencer (Illumina Inc, San Diego, CA) were paired and processed using the MOTHUR pipeline,<sup>10</sup> and the BIOM package<sup>11</sup> was subsequently used to transfer biom files into R software<sup>12</sup> for generating graphs of relative taxa abundance and beta diversity.

## Supplementary References

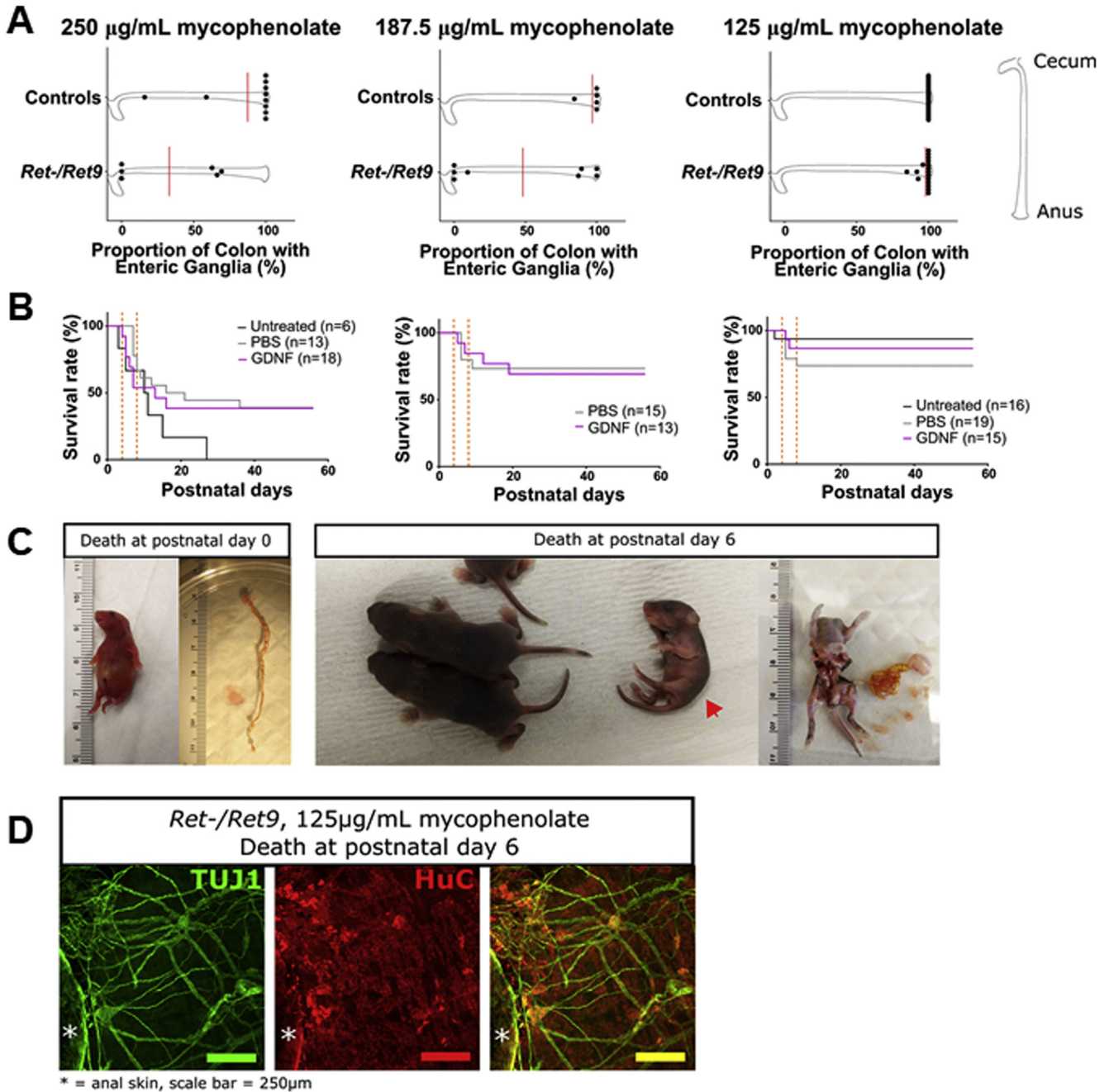
- Bergeron KF, Cardinal T, Toure AM, et al. Male-biased aganglionic megacolon in the TashT mouse line due to perturbation of silencer elements in a large gene desert of chromosome 10. *PLoS Genet* 2015;11:e1005093.
- Pilon N, Raiwet D, Viger RS, et al. Novel pre- and post-gastrulation expression of Gata4 within cells of the inner cell mass and migratory neural crest cells. *Dev Dyn* 2008;237:1133–1143.
- Soret R, Mennetrey M, Bergeron KF, et al. A collagen VI-dependent pathogenic mechanism for Hirschsprung's disease. *J Clin Invest* 2015;125:4483–4496.
- Srinivas S, Watanabe T, Lin CS, et al. Cre reporter strains produced by targeted insertion of EYFP and ECFP into the ROSA26 locus. *BMC Dev Biol* 2001;1:4.
- Enomoto H, Crawford PA, Gorodinsky A, et al. RET signaling is essential for migration, axonal growth and axon guidance of developing sympathetic neurons. *Development* 2001;128:3963–3974.
- Jain S, Naughton CK, Yang M, et al. Mice expressing a dominant-negative Ret mutation phenocopy human Hirschsprung disease and delineate a direct role of Ret in spermatogenesis. *Development* 2004;131:5503–5513.
- Lake JI, Tusheva OA, Graham BL, et al. Hirschsprung-like disease is exacerbated by reduced de novo GMP synthesis. *J Clin Invest* 2013;123:4875–4887.
- Boulende Sab A, Bouchard MF, Beland M, et al. An Ebox element in the proximal Gata4 promoter is required for Gata4 expression in vivo. *PLoS One* 2011;6:e29038.
- Laforest-Lapointe I, Paquette A, Messier C, et al. Leaf bacterial diversity mediates plant diversity and ecosystem function relationships. *Nature* 2017;546:145–147.
- Schloss PD, Westcott SL, Ryabin T, et al. Introducing mothur: open-source, platform-independent, community-supported software for describing and comparing microbial communities. *Appl Environ Microbiol* 2009;75:7537–7541.
- McDonald D, Clemente JC, Kuczynski J, et al. The Biological Observation Matrix (BIOM) format or: how I learned to stop worrying and love the ome-ome. *Gigascience* 2012;1:7.
- Team RCR. A language and environment for statistical computing. Vienna, Austria: R Foundation for Statistical Computing, 2014.
- Chalazonitis A, D'Autreaux F, Guha U, et al. Bone morphogenetic protein-2 and -4 limit the number of enteric neurons but promote development of a TrkC-expressing neurotrophin-3-dependent subset. *J Neurosci* 2004;24:4266–4282.

14. Nagy N, Goldstein AM. Endothelin-3 regulates neural crest cell proliferation and differentiation in the hindgut enteric nervous system. *Dev Biol* 2006;293:203–217.
15. Liu MT, Kuan YH, Wang J, et al. 5-HT<sub>4</sub> receptor-mediated neuroprotection and neurogenesis in the enteric nervous system of adult mice. *J Neurosci* 2009; 29:9683–9699.
16. Fiorica-Howells E, Maroteaux L, Gershon MD. Serotonin and the 5-HT<sub>2B</sub> receptor in the development of enteric neurons. *J Neurosci* 2000;20:294–305.
17. Fattahi F, Steinbeck JA, Kriks S, et al. Deriving human ENS lineages for cell therapy and drug discovery in Hirschsprung disease. *Nature* 2016;531:105–109.

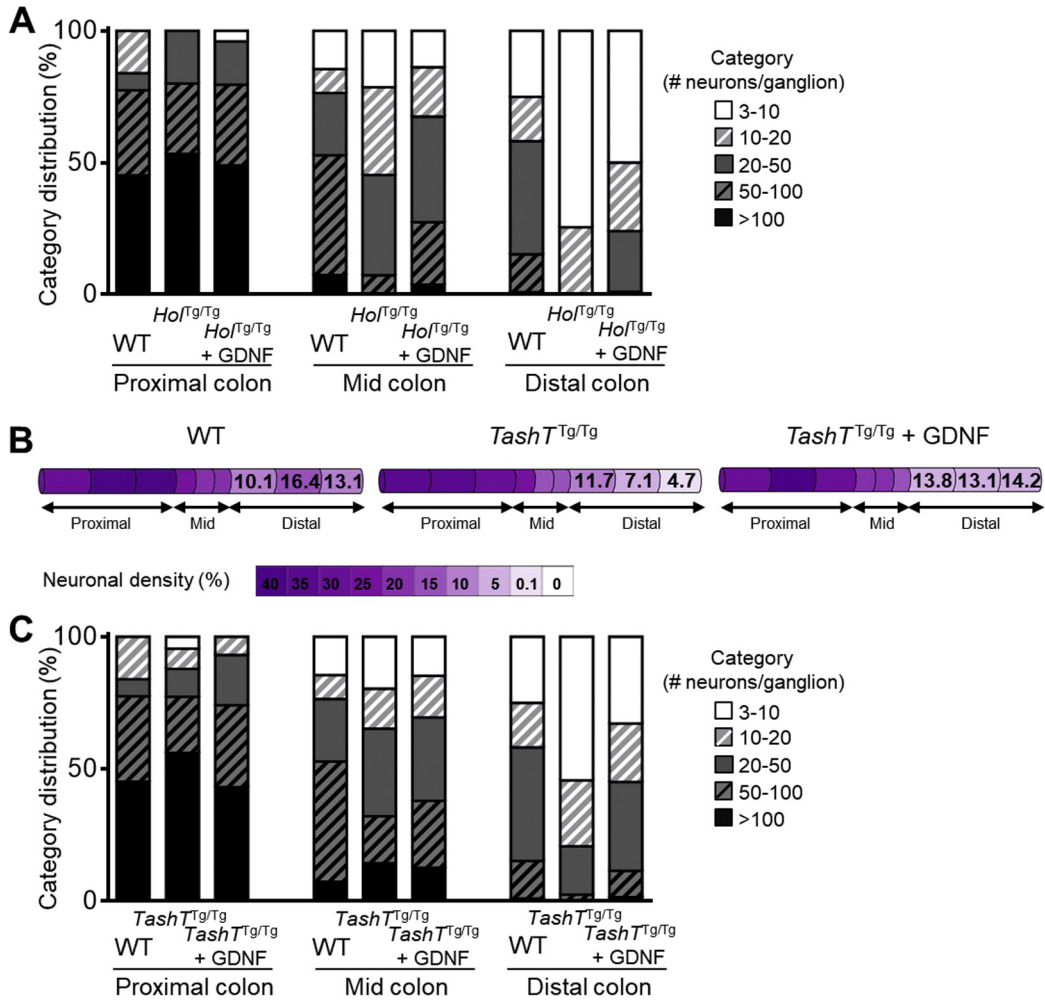


---

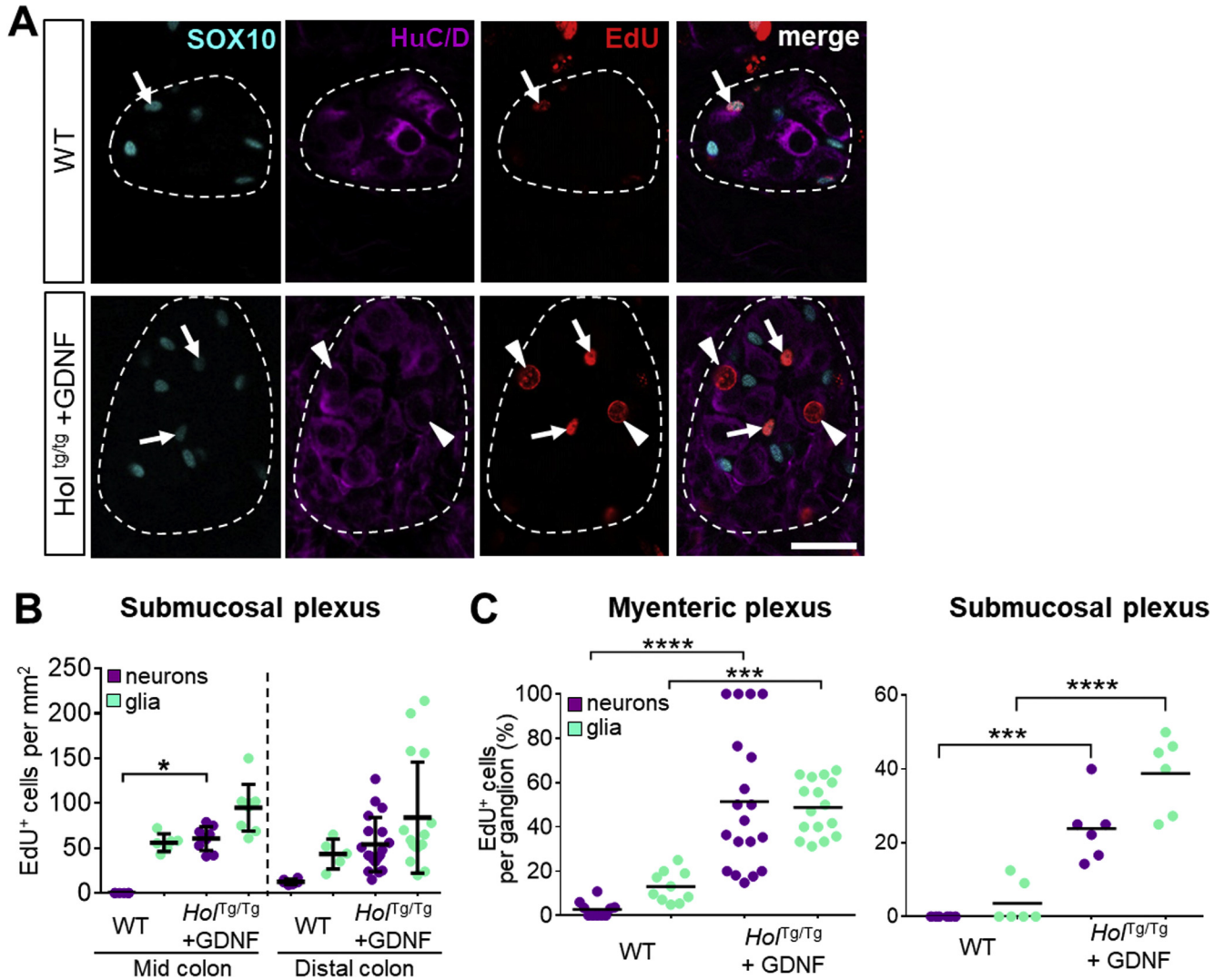
**Supplementary Figure 1.** Setup of GDNF therapy parameters in *Hol<sup>Tg/Tg</sup>* mice. (A) Distribution of 10  $\mu$ L methylene blue enemas in the colon of P4 and (B) P8 *Hol<sup>Tg/Tg</sup>* pups. (C) Age and cause of death of the few GDNF-treated *Hol<sup>Tg/Tg</sup>* mice that were allowed to survive beyond P56. n/a, not available. (D) Impact of GDNF concentration on survival of *Hol<sup>Tg/Tg</sup>* pups that received 10- $\mu$ L enemas once daily between P4 and P8. Indicated amounts correspond to the total quantity of GDNF that was administered each day. (E) Impact of treatment time window (P4–P8 vs P8–P12), duration (1 day, 5 days, or 10 days, starting at P4) and frequency (once or twice a day, for 5 days) on the survival of *Hol<sup>Tg/Tg</sup>* pups treated with GDNF enemas (quantity of GDNF administered per single enema was kept constant at 10  $\mu$ g in 10  $\mu$ L). (F) Survival rate of *Hol<sup>Tg/Tg</sup>* pups that were administered 10- $\mu$ L enemas containing the indicated neurotrophic molecule (Noggin, endothelin-3, or the serotonin receptor agonist RS67506; all at 1  $\mu$ g/ $\mu$ L final concentration) once daily between P4 and P8. (G) Impact of food consistency (regular chow vs gel diet) on survival of *Hol<sup>Tg/Tg</sup>* pups that received GDNF enemas (10  $\mu$ g in 10  $\mu$ L) daily between P4 and P8. (H) Impact of coadministration of ascorbic acid (Vit C; 100  $\mu$ mol/L final concentration), serotonin (5-hydroxytryptamine [5-HT]; 1  $\mu$ g/ $\mu$ L final concentration) and endothelin-3 (ET3; 1  $\mu$ g/ $\mu$ L final concentration) on survival of *Hol<sup>Tg/Tg</sup>* pups that received GDNF enemas (10  $\mu$ g in 10  $\mu$ L) once daily between P4 and P8. (I) Neuron density in the colon (expressed in percentage of surface area) and associated health status of P20 *Hol<sup>Tg/Tg</sup>* mice that received GDNF enemas (10  $\mu$ g in 10  $\mu$ L) daily between P4 and P8.



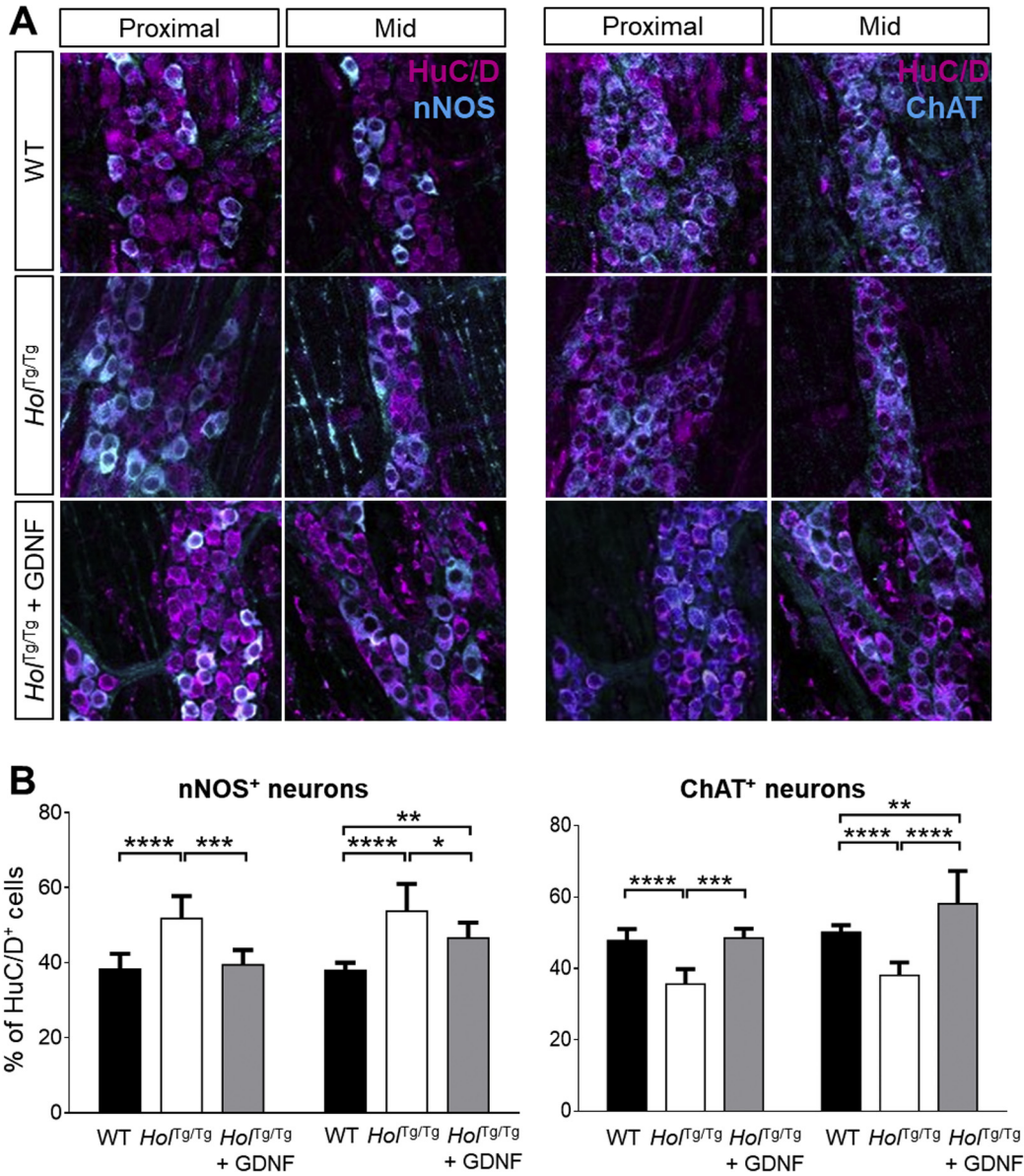
**Supplementary Figure 2.** GDNF enemas do not rescue survival in RET hypomorph mouse model of HSCR. (A) Treatment of pregnant dams with increasing doses of mycophenolate mofetil from E7.5 to E18.5 increases penetrance of HSCR-like aganglionosis and the length of aganglionic bowel in the newborn *Ret*<sup>-9</sup> pups. A few *Ret*<sup>wt/9</sup> littermates (graphed as part of the control group) also exhibited aganglionosis. (B) There is no survival difference for mice treated from P4 to P8 with GDNF vs PBS for all mycophenolate mofetil concentrations. Log-rank test and Gehan-Breslow-Wilcoxon test for all data sets, *P* > 0.1. (C) *Ret*<sup>-9</sup> mice died during the P4 to P8 treatment period with bowel distention. (D) Representative image of the distal colon of 125 µg/mL mycophenolate-treated *Ret*<sup>-9</sup> pups that died during the treatment period. This specific pup died at P6 (as seen in C) even though myenteric neurons (HuC/D<sup>+</sup>) completely colonized the bowel (anal skin marked with \*). Extrinsic nerve fibers are also visualized (TuJ1<sup>+</sup>). Scale bar, 250 µm.



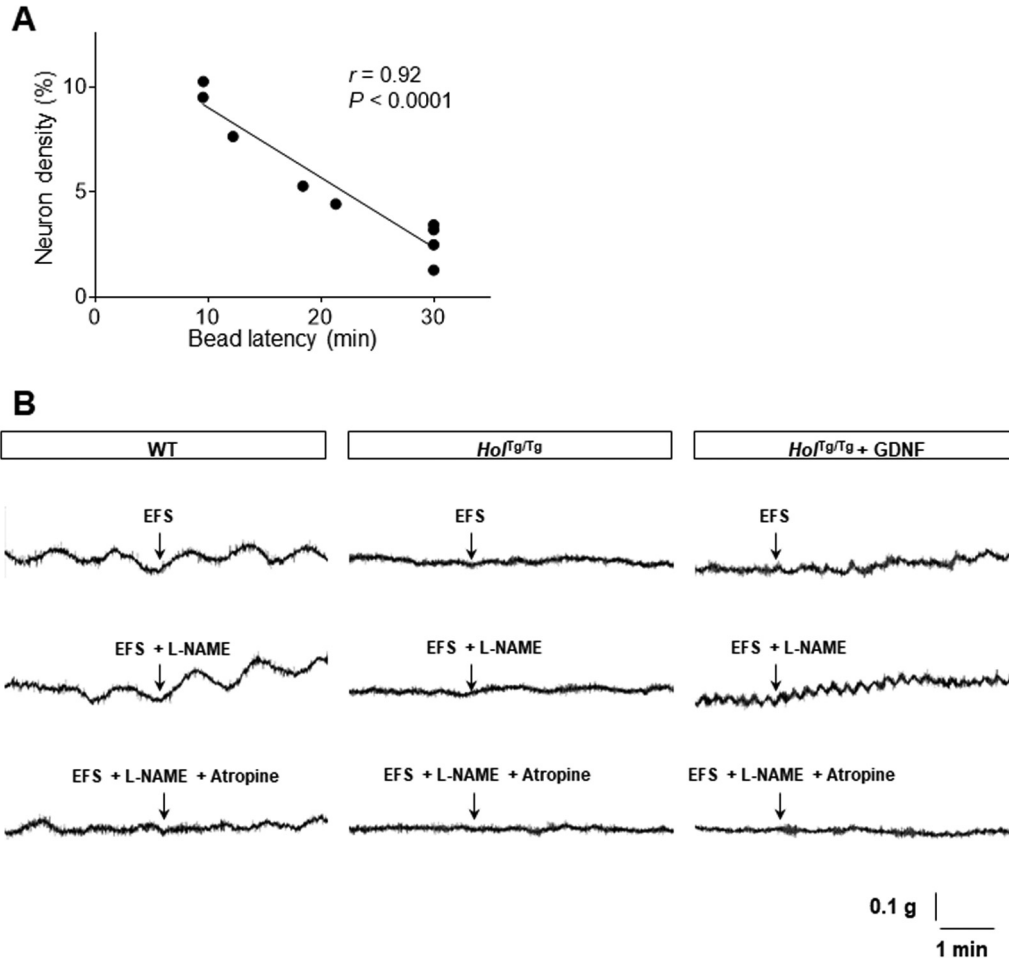
**Supplementary Figure 3.** Analysis of myenteric ganglion size and neuronal density in the colon of P20 *Ho1<sup>Tg/Tg</sup>* and *TashT<sup>Tg/Tg</sup>* mice that were treated or not with GDNF between P4 and P8. (A) Analysis of myenteric ganglion size in *Ho1<sup>Tg/Tg</sup>* mice. (B) Analysis of neuronal density in *TashT<sup>Tg/Tg</sup>* mice. The average neuronal density (color coded) is indicated for each colon subregion (represented by cylinders) along the length of the colon. Neuronal density is expressed as the percentage of area occupied by HuC/D<sup>+</sup> cells in a single focal plane at the level of the myenteric plexus within the bowel wall (n = 6 mice per group; 3 fields of view per subregion). For each distal colon subregion, the neuronal density is also given as a numerical value. (C) Analysis of myenteric ganglion size in *TashT<sup>Tg/Tg</sup>* mice.



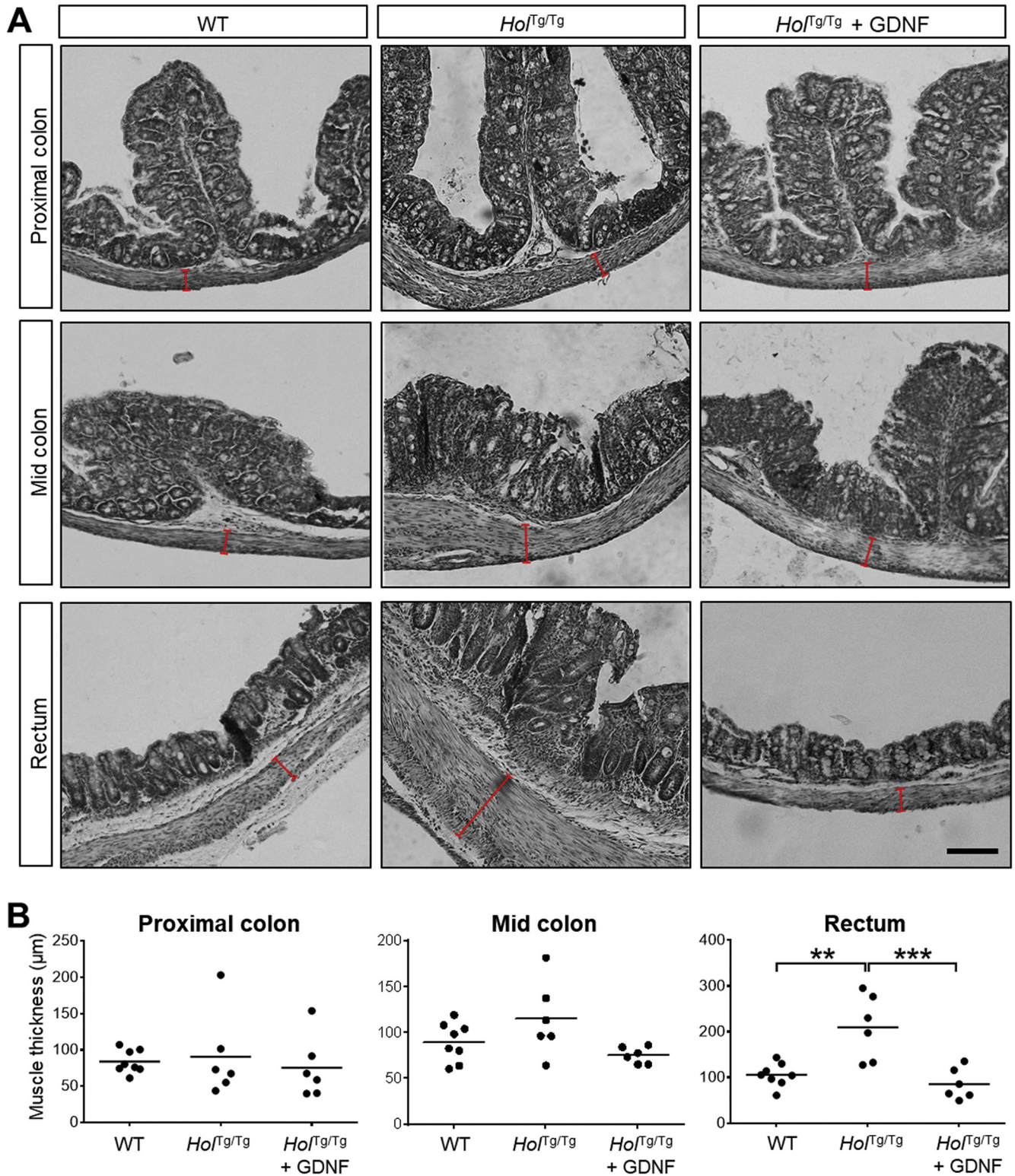
**Supplementary Figure 4.** Analysis of EdU incorporation in myenteric and submucosal ganglia of the colon from P20 WT and GDNF-treated *Ho1<sup>Tg/Tg</sup>* mice that were administered EdU between P4 and P8. (A) Example of EdU incorporation in a z-stack projection of submucosal neurons (arrowheads) and glia (arrows) in the distal colon. The dashed outline marks area occupied by a single ganglion. Scale bar, 50  $\mu$ m. (B) Quantitative analysis of EdU incorporation in submucosal neurons (HuC/D<sup>+</sup>) and glia (SOX10<sup>+</sup>) in the middle and distal colon. Results are expressed as the number of EdU<sup>+</sup> cells/mm<sup>2</sup> (n = 3 WT and 3 GDNF-treated *Ho1<sup>Tg/Tg</sup>* mice; 2–7 fields of view per animal). \**P* < .05; 1-way analysis of variance with post hoc Sidak’s test. (C) Quantitative analysis of EdU incorporation in myenteric (left panel) and submucosal (right panel) neurons (HuC/D<sup>+</sup>) and glia (SOX10<sup>+</sup>) in distal colon. Results are expressed in the percentage of EdU<sup>+</sup> cells per ganglion (n = 3 WT and 3 GDNF-treated *Ho1<sup>Tg/Tg</sup>* mice; 2–7 fields of view per animal). \*\*\**P* < .001; \*\*\*\**P* < .0001; 1-way analysis of variance with post hoc Sidak’s test. GDNF-treated mice received 10  $\mu$ g GDNF in 10- $\mu$ L enemas once daily between P4 and P8.



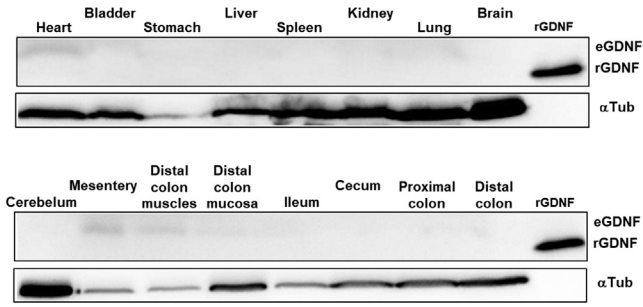
**Supplementary Figure 5.** Proportion of nitrgergic and cholinergic myenteric neurons in the proximal and mid colon of WT, untreated *Ho1Tg/Tg*, or GDNF-treated *Ho1Tg/Tg* mice at P20. (A) Qualitative analysis of the proportion of nitrgergic (left panel) and cholinergic (right panel) neurons. Scale bar, 50  $\mu$ m. (B) Quantitative analysis of the proportion of nitrgergic (left panels) and cholinergic (right panels) neurons (n = 3 WT and 3 GDNF-treated *Ho1Tg/Tg* mice; 3 fields of view per animal). \**P* < .05; \*\**P* < .01; \*\*\**P* < .001; \*\*\*\**P* < .0001; 1-way analysis of variance with post hoc Sidak's test. GDNF-treated mice received 10  $\mu$ g GDNF in 10- $\mu$ L enemas once daily between P4 and P8.



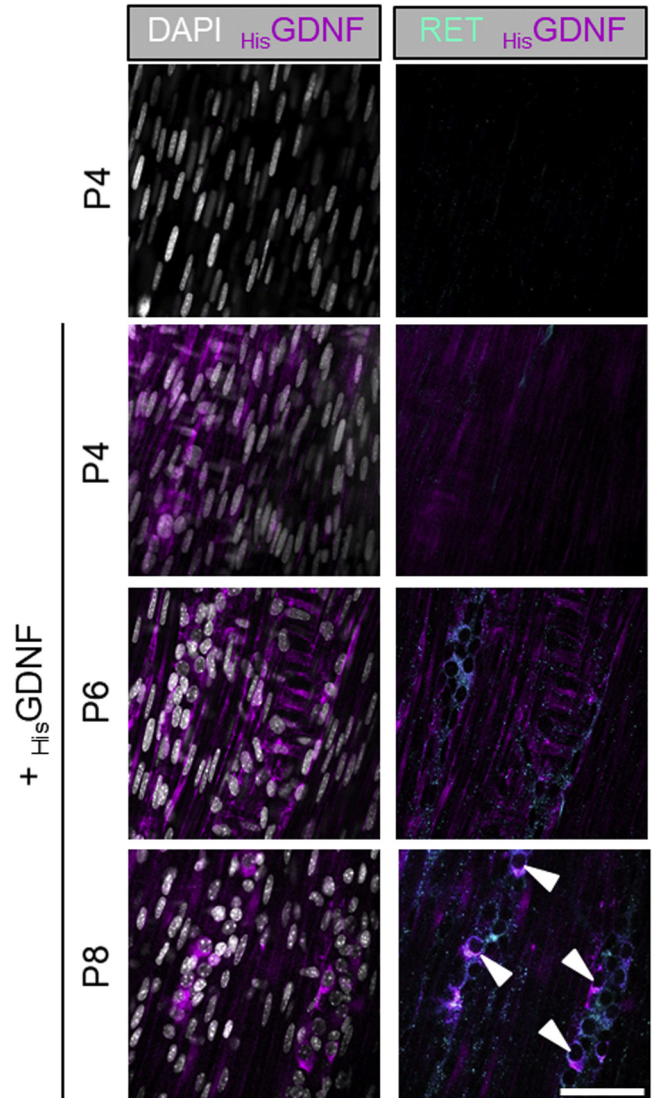
**Supplementary Figure 6.** Supporting information for in vivo and ex vivo analyses of motility in the distal colon of WT, untreated *Ho1<sup>Tg/Tg</sup>*, or GDNF-treated *Ho1<sup>Tg/Tg</sup>* mice at P20. (A) Correlation between neuron density in the distal colon and time for bead expulsion in GDNF-treated *Ho1<sup>Tg/Tg</sup>* mice at P20 (in support of Figure 3D). (B) Examples of electric field-stimulated and drug-modulated patterns of longitudinal smooth muscle contraction-relaxation in an organ bath equipped with a force transducer (in support of Figure 3E). In responsive tissues, EFS triggers contractions of colonic muscles that can be slightly increased by *N*<sup>G</sup>-nitro-L-arginine methyl ester (L-NAME)-mediated inhibition of nitrergic signaling, and robustly counteracted by atropine-mediated inhibition of cholinergic signaling. GDNF-treated mice received 10  $\mu$ g GDNF in 10- $\mu$ L enemas once daily between P4 and P8.



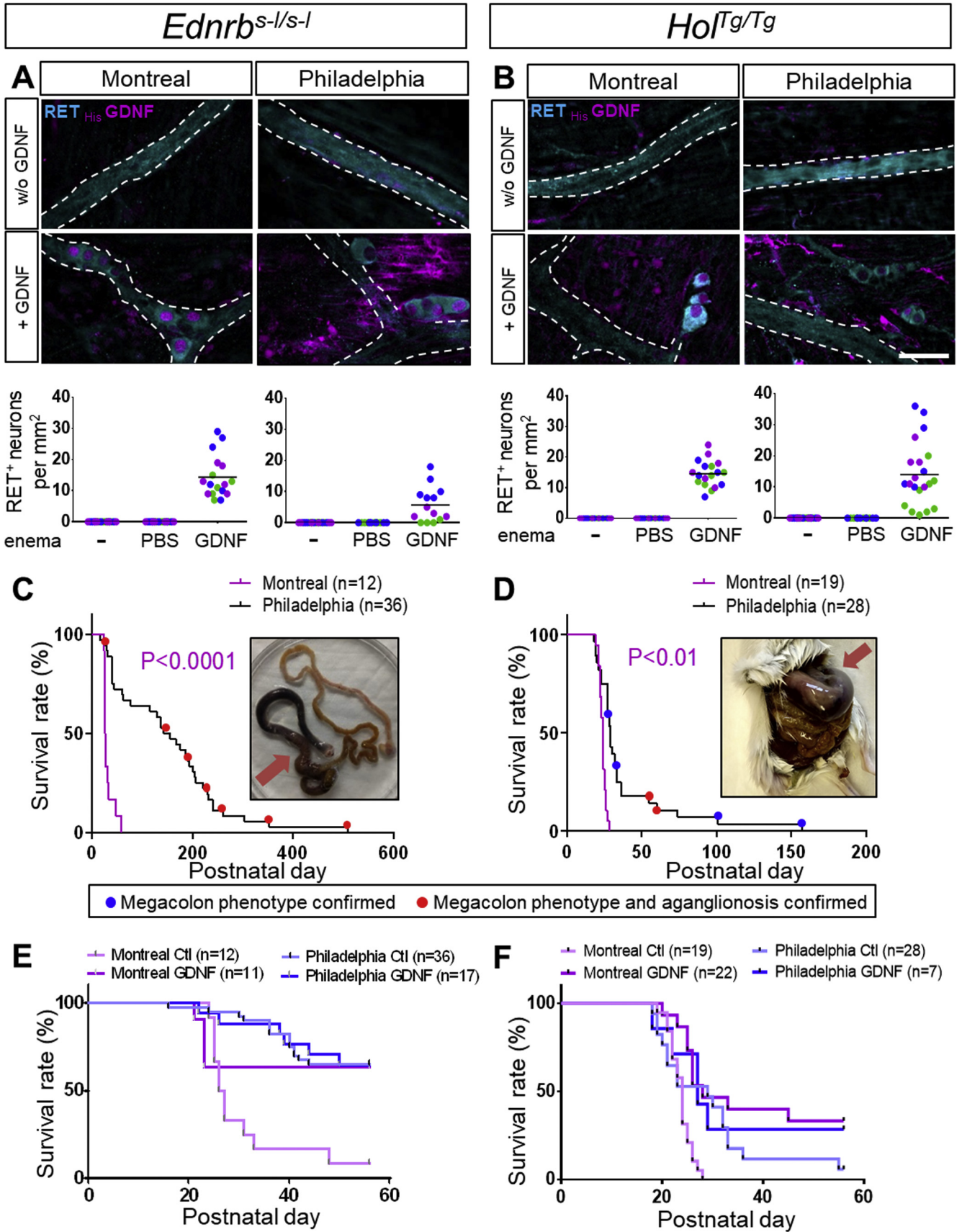
**Supplementary Figure 7.** Analysis of smooth muscle thickness in the distal colon of WT, untreated *Hol<sup>Tg/Tg</sup>*, or GDNF-treated *Hol<sup>Tg/Tg</sup>* mice at P20. (A) Representative H&E-stained cross-sections of different colon segments, with smooth muscle thickness indicated by *red brackets*. Scale bar, 150  $\mu\text{m}$ . (B) Average muscle thickness for each colon segment ( $n = 6$  mice per group).  $**P < .01$ ;  $***P < .001$ ; 1-way analysis of variance with post hoc Tukey's test. GDNF-treated mice received 10  $\mu\text{g}$  GDNF in 10- $\mu\text{L}$  enemas once daily between P4 and P8.

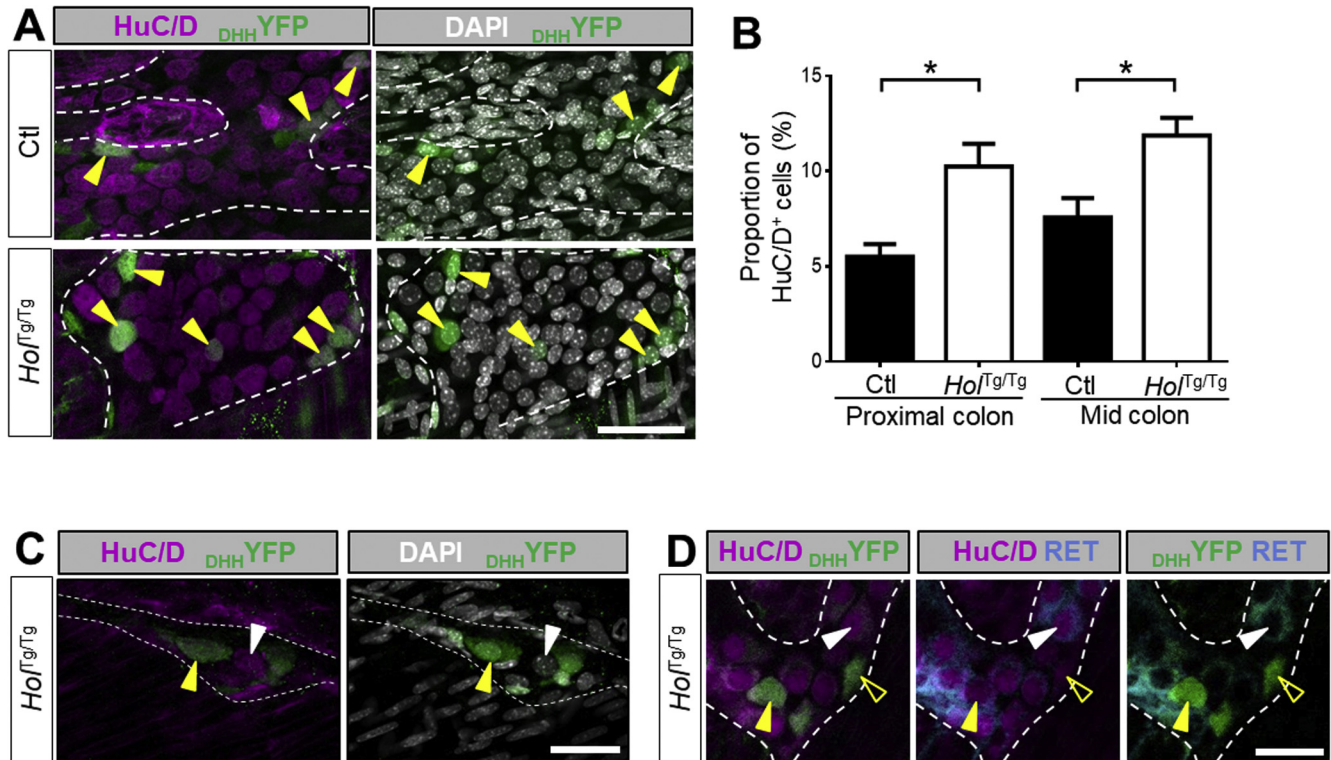


**Supplementary Figure 8.** Analysis of GDNF distribution in multiple tissues of GDNF-treated *Ho1<sup>Tg/Tg</sup>* mice at P20. Western blot analysis of  $\alpha$ -tubulin ( $\alpha$ -Tub)-normalized levels of endogenous GDNF (eGDNF) and recombinant GDNF (rGDNF) in different tissues of P20 *Ho1<sup>Tg/Tg</sup>* mice that received 10  $\mu$ g GDNF in 10- $\mu$ L enemas once daily between P4 and P8. The displayed blots are representative of observations made from 3 mice.



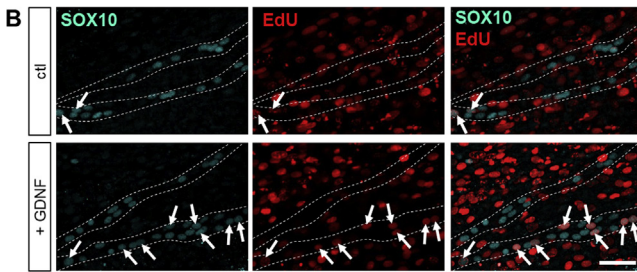
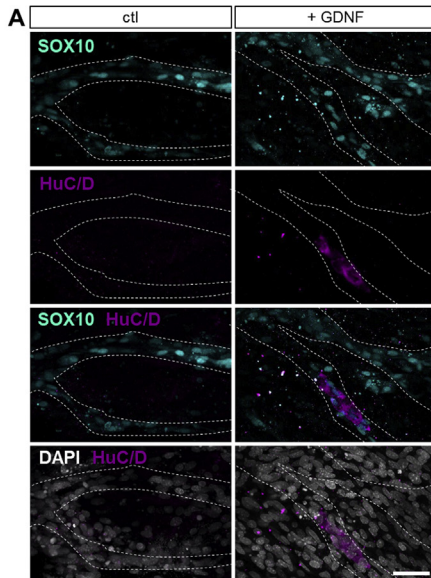
**Supplementary Figure 9.** Time-course analysis of  $_{His}GDNF$  distribution and RET expression in colonic smooth muscles of P4 to P8 *Ho1<sup>Tg/Tg</sup>* mice treated with  $_{His}GDNF$ . Immunofluorescence analysis of  $_{His}GDNF$  distribution and RET expression in distal colon muscularis of  $_{His}GDNF$ -treated *Ho1<sup>Tg/Tg</sup>* mice. The *white arrowheads* point to RET<sup>+</sup> neurons that also stain positive for  $_{His}GDNF$ . All images show a single focal plane representative of observations made from 3 mice. Scale bar, 20  $\mu$ m. DAPI, 4',6-diamidino-2-phenylindole.



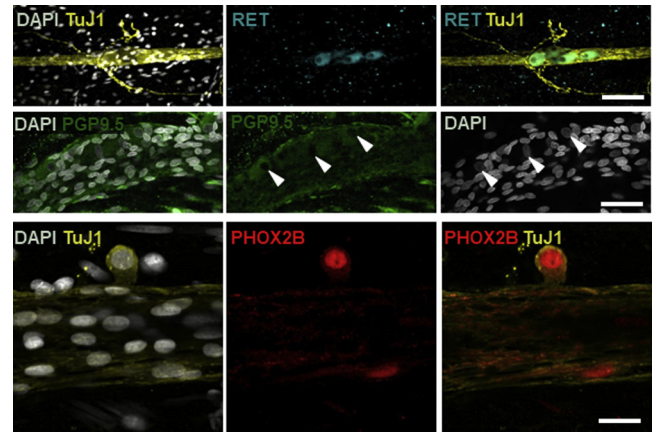


**Supplementary Figure 11.** Analysis of Schwann cell lineage-derived neurogenesis in myenteric and submucosal ganglia of *Dhh-Cre<sup>Tg/+</sup>;R26<sup>YFP/+</sup>* and *Ho1<sup>Tg/Tg</sup>;Dhh-Cre<sup>Tg/+</sup>;R26<sup>YFP/+</sup>* mice at P20. (A) Analysis of myenteric neurons (HuC/D<sup>+</sup>) and YFP expression in the proximal colon of *Dhh-Cre<sup>Tg/+</sup>;R26<sup>YFP/+</sup>* (Ctl) and *Ho1<sup>Tg/Tg</sup>;Dhh-Cre<sup>Tg/+</sup>;R26<sup>YFP/+</sup>* (*Ho1<sup>Tg/Tg</sup>*) mice. The yellow arrowheads point to Schwann cell lineage-derived neurons. (B) Quantitative analyses of myenteric neurons (HuC/D<sup>+</sup>) that are YFP<sup>+</sup> in the proximal and mid colon of *Dhh-Cre<sup>Tg/+</sup>;R26<sup>YFP/+</sup>* (Ctl) and *Ho1<sup>Tg/Tg</sup>;Dhh-Cre<sup>Tg/+</sup>;R26<sup>YFP/+</sup>* (*Ho1<sup>Tg/Tg</sup>*) mice ( $n = 3$  Ctl and 3 *Ho1<sup>Tg/Tg</sup>* mice; 3 fields of view per animal) \* $P < .05$ ; 1-way analysis of variance with post hoc Sidak's test. DAPI, 4',6-diamidino-2-phenylindole. (C) Analysis of submucosal neurons (HuC/D<sup>+</sup>) and YFP expression in the distal colon of *Ho1<sup>Tg/Tg</sup>;Dhh-Cre<sup>Tg/+</sup>;R26<sup>YFP/+</sup>* (*Ho1<sup>Tg/Tg</sup>*) mice that were treated with GDNF between P4 and P8. Neurons of Schwann lineage (yellow arrowhead) or unknown (white arrowhead) origin are detected. (D) Analysis of RET-expressing myenteric neurons (HuC/D<sup>+</sup>) and YFP expression in the distal colon of *Ho1<sup>Tg/Tg</sup>;Dhh-Cre<sup>Tg/+</sup>;R26<sup>YFP/+</sup>* (*Ho1<sup>Tg/Tg</sup>*) mice that were treated with GDNF between P4 and P8. RET is expressed in a subset of neurons, regardless of Schwann cell lineage (RET<sup>+</sup>, filled yellow arrowhead; RET<sup>-</sup>, empty yellow arrowhead) or non-Schwann cell lineage (white arrowhead) origin. All displayed images are z-stack projections representative of observations made from 3 mice. Scale bar, 50  $\mu$ m. The dashed outline marks area occupied by a single ganglion.

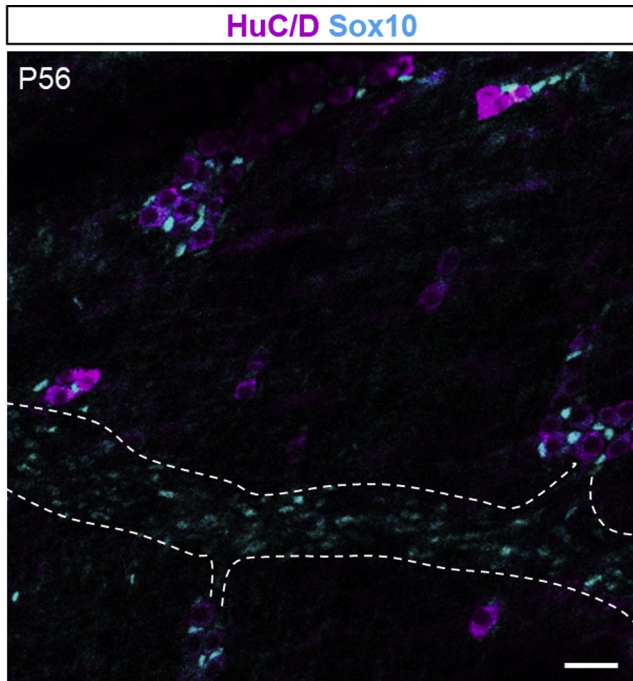
**Supplementary Figure 10.** GDNF enemas trigger enteric neurogenesis without prolonging already extended survival of HSCR mouse models in Philadelphia. In both Montreal and Philadelphia, daily administration of HisGDNF enemas (10  $\mu$ g HisGDNF in 10  $\mu$ L of PBS) between P4 and P8 trigger enteric neurogenesis in both (A) *Ednrb<sup>s-/s-</sup>* and (B) *Ho1<sup>Tg/Tg</sup>* mice (in support of Figure 4C). Upper panels are representative images of immunolabeled distal colons (last cm) at P8 showing the presence of RET and HisGDNF double-positive myenteric neurons close to an extrinsic nerve fiber (dashed outlines). Scale bar, 50  $\mu$ m. Lower panels are quantitative analyses with results expressed in number of RET<sup>+</sup> myenteric neurons per mm<sup>2</sup>. Each dot corresponds to a field of view, with color code meaning that samples were from the same animal ( $n = 3$  for GDNF enemas;  $n = 2$  for untreated and PBS enemas; 4–8 fields of view per animal). Untreated (C) *Ednrb<sup>s-/s-</sup>* (D) and *Ho1<sup>Tg/Tg</sup>* mice live longer in Philadelphia than in Montreal. For many mice that were found dead, megacolon phenotype (distended feces-filled colon, as shown in insets) was visually confirmed (marked by red dots). In addition, some moribund mice were euthanized to prevent colon tissue alteration, thereby allowing confirmation of distal aganglionosis by HuC-TuJ1 double-immunofluorescence (marked by blue dots). For both (E) *Ednrb<sup>s-/s-</sup>* and (F) *Ho1<sup>Tg/Tg</sup>* mice, GDNF treatment in Montreal increases survival to rates seen in untreated mice in Philadelphia ( $P > .5$  for GDNF-treated *Ednrb<sup>s-/s-</sup>* mice in Montreal vs untreated *Ednrb<sup>s-/s-</sup>* mice in Philadelphia.  $P > .7$  for GDNF-treated *Ho1<sup>Tg/Tg</sup>* mice in Montreal vs untreated *Ho1<sup>Tg/Tg</sup>* mice in Philadelphia). GDNF treatment did not further enhance the survival advantage of *Ednrb<sup>s-/s-</sup>* and *Ho1<sup>Tg/Tg</sup>* mice in Philadelphia ( $P > .9$  for untreated *Ednrb<sup>s-/s-</sup>* mice in Philadelphia vs GDNF-treated *Ednrb<sup>s-/s-</sup>* mice in Philadelphia;  $P > .5$  for untreated *Ho1<sup>Tg/Tg</sup>* mice in Philadelphia vs GDNF-treated *Ho1<sup>Tg/Tg</sup>* mice in Philadelphia). Log-rank (Mantel-Cox) and Gehan-Breslow-Wilcoxon tests.



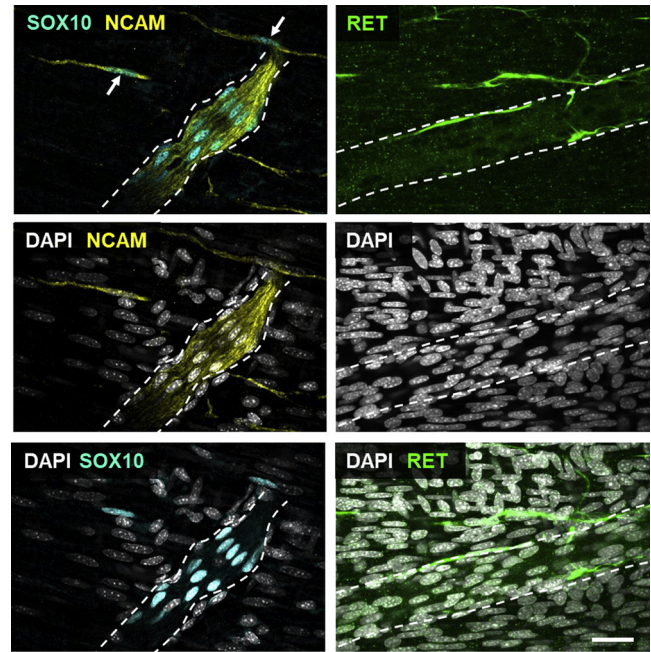
**Supplementary Figure 12.** Analysis of neurogenesis and Schwann's cell proliferation in distal colon explants prepared from P4 *Hoi<sup>Tg/Tg</sup>* mice and cultured in the presence or absence of GDNF for 96 hours. Representative images of (A) HuC/D<sup>+</sup> neurons, and (B) EdU<sup>+</sup> SOX10<sup>+</sup> proliferating Schwann cells (arrows) in explants of distal colon from *Hoi<sup>Tg/Tg</sup>* mice cultured in presence of GDNF and EdU (+GDNF) or EdU alone (ctl). The displayed images are single focal planes representative of observations made from 7 mice. Scale bar, 50  $\mu$ m. The dashed outline marks the area occupied by extrinsic nerve fibers.



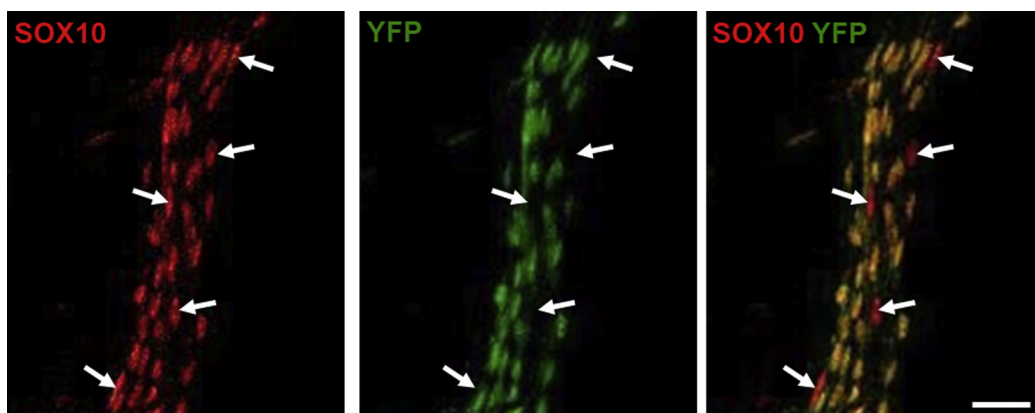
**Supplementary Figure 13.** Marker analysis of GDNF-induced neurons in sigmoid colon explants prepared from HSCR patients and cultured in the presence of GDNF for 96 hours. Immunofluorescence analysis showing that human GDNF-induced neurons are closely associated with extrinsic nerves and express  $\beta$ III-tubulin (TuJ1), RET, PGP9.5, and PHOX2B (in support of Figure 5F). DAPI, 4',6-diamidino-2-phenylindole. The arrowheads in the middle panels point to round/ovoid nuclei of PGP9.5<sup>+</sup> neurons. The displayed images are single focal planes representative of observations made from 3 human samples. Scale bar, 100 $\mu$ m (upper panels), 50  $\mu$ m (middle panels), and 25  $\mu$ m (lower panels).



**Supplementary Figure 14.** GDNF-induced myenteric ganglia are self-sustaining until adulthood. Immunofluorescence analysis of HuC/D and SOX10 expression in myenteric ganglia from the distal colon of GDNF-treated *Hol<sup>Tg/Tg</sup>* mice at P56. The displayed image is a single focal plane representative of observations made from 3 mice. Scale bar, 50  $\mu$ m.



**Supplementary Figure 15.** Schwann cells in the aganglionic distal colon of *Hol<sup>Tg/Tg</sup>* mice express neural cell adhesion molecule (NCAM) but not RET. Immunofluorescence analysis of NCAM and RET expression in extrinsic nerve fibers (delineated by *dashed lines*) from the distal colon of untreated *Hol<sup>Tg/Tg</sup>* mice at P20. NCAM but not RET is expressed in SOX10<sup>+</sup> Schwann cells and putative enteric glia/ENS progenitors (*arrows*). DAPI, 4',6-diamidino-2-phenylindole. The displayed images are single focal planes representative of observations made from 3 mice. Scale bar, 50  $\mu$ m.



**Supplementary Figure 16.** Schwann cells in the aganglionic distal colon of *Hol<sup>Tg/Tg</sup>;Dhh-Cre<sup>Tg/+</sup>;R26<sup>YFP/+</sup>* mice are not all YFP-labeled. Immunofluorescence analysis of SOX10 and YFP expression in an extrinsic nerve fiber from distal colon of untreated *Hol<sup>Tg/Tg</sup>;Dhh-Cre<sup>Tg/+</sup>;R26<sup>YFP/+</sup>* mice at P8. A subset of SOX10<sup>+</sup> Schwann cells are negative for YFP (*arrows*). The displayed images are single focal planes representative of observations made from 3 mice. Scale bar, 50  $\mu$ m.

**Supplementary Table 1.** Rationale for Selection of Supplemental Neurotrophic Molecules

Molecule	Reason for selecting	Reference
Noggin	NSE promoter-driven Noggin overexpression increases enteric neuron numbers in transgenic mice	Chalazonitis et al, <i>J Neurosci</i> 2004 <sup>13</sup>
Endothelin-3	Ex vivo culture of avian hindgut in presence of endothelin-3 increases ENS density	Nagy and Goldstein, <i>Dev Biol</i> 2006 <sup>14</sup>
RS67506	Systemic administration of the serotonin receptor (5-HT4R) agonist RS67506 triggers enteric neurogenesis in adult mice	Liu et al, <i>J Neurosci</i> 2009 <sup>15</sup>
Serotonin	Serotonin (5-HT) enhances in vitro neuronal differentiation of murine enteric neural precursors	Fiorica-Howells et al, <i>J Neurosci</i> 2000 <sup>16</sup>
Vitamin C	Ascorbic acid is needed for in vitro differentiation and maturation of human enteric neural precursors	Fattahi et al, <i>Nature</i> 2016 <sup>17</sup>

NSE, neuron-specific enolase; 5-HT, 5-hydroxytryptamine; 5HT4, 5-hydroxytryptamine receptor 4.

**Supplementary Table 2.** List of Primary Antibodies and Dilution Factors Used for Immunofluorescence

Antibody	Source <sup>a</sup>	Catalog number	RRID reference	Dilution
His tag	R&D Systems	MAB050	AB_357353	1:500
calretinin	Swant	CG1	AB_10000342	1:500
choline acetyltransferase	Millipore	AB144P	AB_2079751	1:100
green fluorescent protein	Abcam	Ab290	AB_303395	1:500
HuC/D	Molecular Probes	A-21271	AB_221448	1:500
HuC/D (ANNA-1)	Gift from Vanda Lennon	...	AB_2313944	1:2000
Ki67	Abcam	ab15580	AB_443209	1:500
neural cell adhesion molecule	Abcam	ab5032	AB_2291692	1:500
NOS1	Santa Cruz Biotechnology	sc-648	AB_630935	1:200
PHOX2B	R&D Systems	AF4940	...	1:250
RET	R&D Systems	MAB718	AB_2232594	1:500
SOX10	Santa Cruz Biotechnology	sc-17342	AB_2195374	1:200
substance P	Abcam	ab67006	AB_1143173	1:500
tyrosine hydroxylase	Abcam	ab137869	...	1:500
betalll tubulin (Tuj1)	Covance	MRB-435P	AB_663339	1:1000
vasointestinal peptide	Abcam	ab8556	AB_306628	1:500

RRID, Research Resource Identifiers

<sup>a</sup>Swant, Marly, Switzerland; Molecular Probes, Eugene, Oregon; Vanda Lennon, Mayo Clinic, Rochester, Minnesota; Covance, Princeton, New Jersey.